Tuning the Luminescence of Phosphors: Beyond Conventional Chemical Method

*Gongxun Bai, Ming-Kiu Tsang, and Jianhua Hao**

Tuning the luminescence of phosphors is extremely important in controlling and processing light for active components of light sources, optical sensing, display devices, and biomedicine. So far, conventional chemical approaches have routinely been employed to modify the luminescence during the phos- phor's synthesis. It is interesting to broaden the modulation of luminescence by physical methods, such as electric field, magnetic field, mechanical stress, temperature, photons, ionizing radiation, and so on. Since some physical methods may provide unusual routes to tune the luminescence in in-situ, real-time, dynamical and reversible manners, it should be beneficial for our understanding the fundamentals of luminescence and widespread applica- tions in a variety of advanced optical materials and devices. In this review, a unified picture and primary physical strategies used for tuning the lumines- cence are provided. An attempt is made to review recent advances of tuning the luminescence in a wide range of phosphors, including metal-ion-doped compounds, semiconductors, 2D layered nanomaterials, and stimuli-respon- sive organic phosphors. Lastly, some potential directions of challenging issues in this exciting field are suggested.

1. Introduction

Phosphor, also called a luminescent material, is a substance that emits light, or luminescences, when excited by some kinds of external energy. Here light includes not only electromagnetic waves in the visible region between 390 and 700 nm but also those in the nearby regions on both ends, such as ultraviolet (UV) and near-infrared (NIR) spectra.[1] Considering the com- position and luminescence mechanism, phosphors can be classified into several types, including metal-ion-doped phos- phors, semiconductors, organic phosphors, ionic crystal, etc. Depending on the sources of excitation, luminescence can be classified as photoluminescence (PL), mechanoluminescence (ML), cathodoluminescence (CL), electroluminescence (EL), thermoluminescence (TL), and so on.[2] Nowadays, a large number of phosphors have been synthesized and developed, each one having its own characteristic emission wavelength, bandwidth, and luminescence lifetime. Here, the lifetime normally means the time in which the emission intensity decays to 1/*e*. Moreover, phosphors have been extensively utilized in many areas, both scientific research and practical applications. For instance, phosphor-converted fluorescent lamps and white light-emitting devices (LEDs) have been used as light sources in a widespread range of daily life and industrial applica- tions.[3] CL and EL phosphors have been applied to traditional or modern display devices presenting visual information.[4] In the past few decades, fluorescent nanopar- ticles, such as quantum dots (QDs)[5] and lanthanide (Ln) ion-doped nanocrystals,[6] have attracted considerable attention and showed great promise in fluorescent probes, biosensing, bioimaging, therapies, and optoelectronic devices.[7]The ability to tune the luminescence properties of phosphors is highly desired in the optical materials community.[8] For var- ious applications such as solid-state lasers, bioimaging, optical sensing, and display devices, precise control over the lumines- cence properties is essential for optimizing the performance and processing of optical devices and systems. Tuning lumi- nescence is also of great significance for fundamental studies of the luminescence mechanisms of phosphors. In general, tuning luminescence in the visible region is popularly known as varying the emission colour and brightness obtained by the naked eye. Broadly speaking, tuning luminescence changes the emission intensity, wavelength, bandwidth, luminescence decay or lifetime, and polarization.

Numerous studies have extensively focused on tuning the luminescence of phosphors by conventional chemical ways, typically changing chemical compositions, crystal structure, phase, nanocrystal size, surface groups, and so on.[9] Compara- tively, there have been less results that show the tunable lumi- nescence of phosphors through physical methods. So far, few attempts have been made to provide a comprehensive coverage of the strategies pertaining to this emerging research field and a broad overview of research advances in diverse areas of appli- cation. In this review, chemically driven luminescence tuning is briefly described first so as to make a comparison with tunable luminescence by physical methods, which is described in sub- sequent sections. After that, we present the fundamentals and principles of tuning the luminescence of phosphors beyond chemical methods. According to the introduced strategies of physical methods in Section 3, various applications of lumines- cence tuning are highlighted from Section 4 to Section 6 based on different groups of phosphors, including metal-ion-doped phosphors, semiconductors, atomic-layered 2D nanomaterials, and stimuli-responsive organic phosphors. Finally, we conclude with perspectives.

2. Tuning the Luminescence by a Chemical Method

Before introducing the tuning of luminescence by physical methods, we briefly present conventional chemical methods used for modulation. In principle, tuning the luminescence of phosphors through chemical routes is usually achieved in the synthesis process.[10]

2.1. Chemical Composition-Induced Tuning

Note that a large group of widely used luminescent materials are so-called metal-ion-doped phosphors, where dopants (activators and sensitizers) and a suitable host are composed.[11] A change in the kind and concentration of activator is known to be the simplest way to realize tunable luminescence, as different activators absorb the supplied energy and then emit specific light due to the variation in the energy-level structure of the activators. In addition, co-doping sensitizers can improve the efficiency of absorption and emission through energy transfer. Taking Ln ion-doped phosphors as examples, because of the parity-forbidden nature of the intraconfigurational transition of Ln^{3+} ions, Yb^{3+} ions are doped into the host matrixes for efficient luminescence due to their large absorption cross section in the NIR.[12] Thus, Yb^{3+} ions as sensitizers are usually co-doped with Er^{3+}, Tm^{3+}, and Ho^{3+} activator ions to enhance the luminescence.[13] **Figure 1**a shows ZnO:RE (RE = Eu, Er, and Tm) thin films with multicolor EL by doping different RE activators.[14] Through co-doping sensitizer Yb^{3+} ions and activator Tm^{3+} ions with varied concentrations into nanocrystals, tunable lifetimes are achieved owing to energy transfer across varying sensitizer–activator distances.[15] Tunable luminescence induced by host composition has also been observed in metal-ion-doped optical materials. For example, transition metal Ni^{2+}-doped transparent glass ceramics containing nanocrystals of different compositions exhibit a dissimilar emission peaks, owing to the change in coordination, active ion–anion distances and angles.[16] Through chemical substitution of Ba to Sr in ferroelectric oxides (Figure 1b),[17] leading to the variation in the crystal field around activators, the NIR luminescence properties of Ni^{2+} can be finely tuned, including bandwidth, PL intensity, emission peak position, and luminescence decay. More importantly, such an approach of chemical substitution is very effective, and the emission wavelength shift can exceed 269 nm.

Semiconductors containing electronic band structures are another important group of phosphors. In general, the luminescence of a semiconductor originates from the free-carrier and exciton recombination. The emission wavelength is dependent on the energy bandgap between the valence or exciton band and conduction band. As the bandgap is associated with the composition of the semiconductor, luminescence can

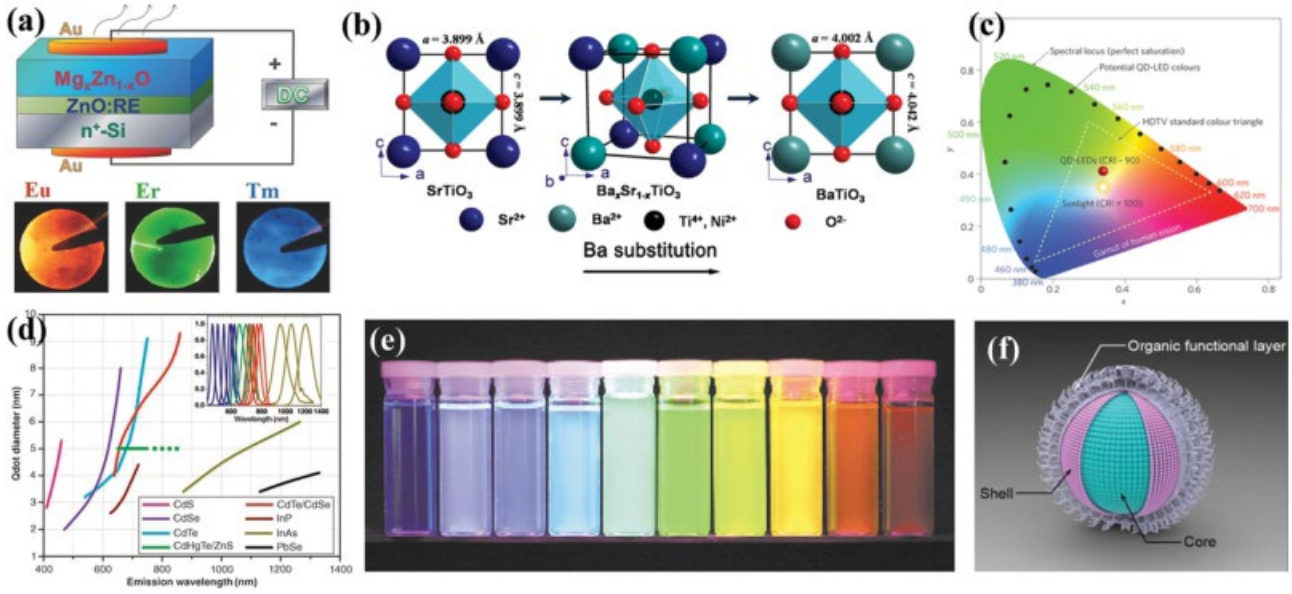

Figure 1. Tuning the luminescence of phosphors by a conventional chemical method. a) The LED utilizing ZnO:RE thin films with multicolour emission, RE = Eu, Er, and Tm, respectively. Reproduced with permission.[14] Copyright 2014, John Wiley & Sons, Inc. b) Crystal structures of Ni^{2+}-doped perovskite $Ba_xSr_{1-x}TiO_3$, with chemical substitution. Reproduced with permission.[17] Copyright 2014, The Royal Society of Chemistry. c) The potential QD-LED colours enable a large colour gamut in the Commission Internacionale d'Éclairage (CIE) diagram. Reproduced with permission.[21] Copyright 2012, Nature Publishing Group. d) Emission lines and sizes of QDs with different compositions. Inset: Representative PL spectra for some QD phosphors. Reproduced with permission.[25] Copyright 2005, American Association for the Advancement of Science. e) ZnS-capped CdSe QDs display ten distinctive colours excited with a UV lamp. Reproduced with permission.[27] Copyright 2001, Nature Publishing Group. f) Schematic illustration of core–shell QD structure with ligands. Reproduced with permission.[33] Copyright 2012, Ivyspring International Publisher.

be tuned through changing the chemical formula of the semiconductor.[18] For example, with an increase in Zn concentration, $Zn_xCd_{1-x}Se$ (0 δ *x* δ 1) nanocrystals exhibit a systematic blueshift in the visible emission spectra because of the broadening bandgap.[19] As Cd content in $Zn_xCd_{1-x}S$ nanoribbons increases, the near-bandgap emission shows a redshift from 340 (pure ZnS) to 515 nm (pure CdS).[20] More importantly, benefiting from the development of semiconductor materials with variable composition and LED technology, modern LEDs that can emit tunable colours are used in a wide-spread range of applications. According to Figure 1c, with the spectral purity of QD emitters, it is possible to select multicolour QD-LED sources whose colour gamut is larger than the International Telecommunication Union High-definition Television (HDTV) standards.[21]

The variation of dopants and composition can also adjust the spin singlet or triplet states in organic luminescence materials, which causes modulation of the luminescence.[22] One typical example is that the EL colours and intensity of organic thin films (8-hydroxyquinoline aluminum) can readily be tuned by choosing a suitable dopant as well as by altering the doping concentration.[23] By varying the chemical composition of organic crystals, the emission colour can be tuned due to the difference in the electron density of the chromopore and the triplet level.[24]

2.2. Nanocrystal Size and Core–Shell Structure-Induced Tuning

Besides changing the chemical formula of phosphors, the manipulation of the size and structure of nanocrystals can achieve tailorable emission. As is well known, the crystalline sizes of nanostructured phosphors play an important role in optical tuning. For QDs, due to quantum confinement, the effective bandgap expands when decreasing the nanocrystal size. Thus, a decrease in the sizes of QDs may result in a blueshift of the emission wavelength. As shown in Figure 1d, QDs with different compositions have both composition- and size-dependent emissions.[25] For instance, small CdSe QDs (diameter 2.3 nm) exhibit blue light under optical excitation, whereas their larger dots (diameter 5.5 nm) give red emission.[26] By controlling particle size, ZnS-capped CdSe QDs display ten distinct colours under UV excitation (Figure 1e).[27]

In general, the concentrations of surface defects increase as the size of the nanostructured phosphors decreases.[28] Moreover, those defects act as surface quenching sites and those emissions that require more phonons to bridge the energy gaps are readily susceptible to the defects. Taking upconversion nanocrystals as examples, the blue emission relative to NIR upconversion emission of Tm^{3+} ions was reduced when the crystalline size became smaller.[29] Similar observations have been reported in Y_2O_3:Yb/Er and $NaYF_4$:Yb/Er upon increasing crystalline size; the ratio of green and red emissions was enhanced due to less quenching effect in green emission that requires more phonons.[30] Alongside this, an enhancement factor of about 30-fold in luminescence intensity was obtained in $NaYF_4$:Yb/Tm@$NaYF_4$ core–shell nanoparticles.[31] For active shells, tuning luminescence mediated by energy migration is developed through the sublattice in $NaGdF_4$:Yb/Tm@$NaGdF_4$:X^{3+} (X = Dy, Sm, Eu, and Tb) core–shell nanoparticles.[32] Similar to this approach, the core–shell structure

of QDs was proposed to enhance the luminescence intensity by epitaxially growing a thin nanocrystalline shell layer (several nanometers) of shell material on the surface of the core nanostructure (Figure 1f).[33] Therefore, the PL quantum yields (QYs) of QDs can be effectively improved by overcoating a thin nanocrystallite with a higher bandgap material which passivates surface nonradiative recombination sites. Up to now, numerous types of core–shell QD structures have been developed, such as CdSe/ZnS,[34] CdSe/ZnSe,[35] CdSe/CdS,[36] CdS/ZnS,[37] and Si/SiO_2[38] core–shell structures.

2.3. Ligand and Surface-Induced Tuning

The aforementioned chemical tuning methods focus on the intrinsic properties of phosphors; one can further tune the luminescence of phosphors by modifying their surface properties, such as capping organic ligands (Figure 1f).[33] Previously, tunable phase structures and luminescence were observed within polyethylene glycol (PEG)-, polyethyleneimine (PEI)-, and 3-mercaptopropionic acid (3MPA)-capped $NaGdF_4$:Yb/Er phosphors under fixed doping compositions.[39] The luminescence tuning effect was explained by controlled nonradiactive decay due to the capping ligands and phase properties. A simple route to tuning the luminescence was explored by controlling the ratio of three types of reactants in thermal decomposition synthesis, namely octadecylamine (OM), oleic acid (OA), and *N*-octadecyloleamide (OOA).[40] Surface ligands are capable of modifying not only the wavelength of upconversion emission but also the emission intensity. Riman and co-workers showed that surfactants could enhance emission intensity by reducing reflection loss at the particle–air interface.[41] They recorded an emission intensity enhancement of five times in polyvinylpyrrolidone (PVP)-modified $NaYF_4$:Yb/Er nanoparticles relative to that with no modification. When surface materials are in close proximity with nanoparticles, the overlapping of the emission with the absorption spectra of the surface materials may facilitate energy transfer, giving rise to the wavelength tuning. For example, emission colour tuning from green to pink is reported in a nanoheterostructure based on CdSe QDs/$NaYF_4$:Yb/Er nanoparticles.[42]

3. Strategies beyond a Chemical Method

Although it is normally effective to modify the luminescence by a chemical approach, chemically driven tuning is essentially an ex-situ and irreversible process. Hence it is unlikely to be able to understand the kinetic process of how the luminescence changes with structural symmetry, crystal field, or band energy through the conventional chemical way. Furthermore, it is almost impossible to isolate the pure crystal-field effect from other extrinsic effects present in different samples of metal-ion-doped phosphors, such as chemical defects and inhomogeneities. Therefore, it is necessary to find an alternative approach to vary the phosphor's energy-level structure and coordination environment in a single material, where tunable luminescence can be achieved. This study is also motivated by the development of multifunctional and on-wafer devices. So far, several

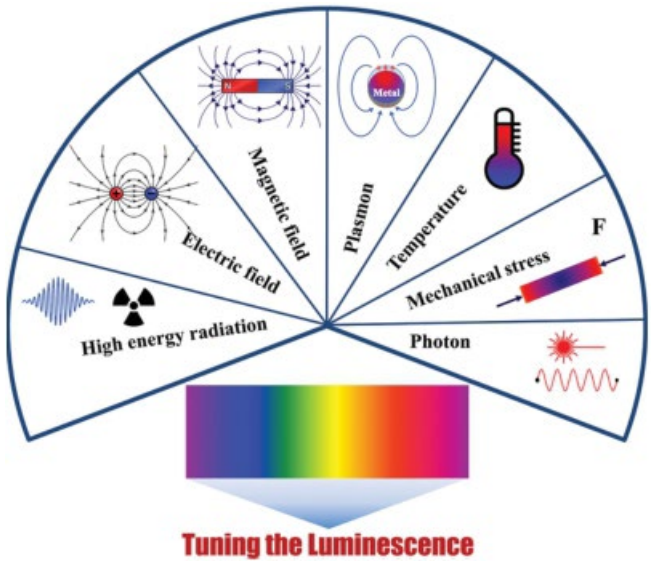

Figure 2. Tuning the luminescence of phosphors: beyond conventional chemical methods.

physical methods have been proposed and demonstrated to modulate the energy-level structure and coordination environment in phosphors.[43] For instance, various external physical stimuli, such as electric fields, magnetic fields, plasmons, photons, mechanical stress, temperature, and ionizing radiation, can be utilized to affect the properties of phosphors, and the related luminescence characteristics can be modulated accordingly (**Figure 2**). In this section, we attempt to introduce the fundamental science of some common strategies for luminescence modification based on the above physical stimuli.

3.1. Electric Field-Induced Tuning

It is well known that an external electric field can cause the splitting and shifting of spectral lines of atoms and molecules; this is denoted the Stark effect.[44] The external electric field tends to shift electrons to the anode and pull nuclei or holes to the cathode. Consequently, an electric-field-induced charge distribution may lead to an additional distortion of energy levels and luminescence shifting. Additionally, the external electric-field-induced Stark effect can cause the splitting of degenerate energy levels, which leads to the splitting of spectral lines. Particularly, the luminescence of semiconductor nanostructures, such as QDs, quantum rods (QRs), and quantum wells (QWs), can be dramatically tuned by an external electric field due to the quantum-confined Stark effect.[45] When applying an electric field to a semiconductor nanostructure, the hole and electron that form the exciton are shifted to opposite sides, but they remain confined in the small bandgap material. Therefore, the exciton is not merely pulled apart by the electric field. Then the light-emission frequency and recombination efficiency could be significantly modulated. For instance, by applying a QD in an external uniform electric field F with the positive direction of z-axis, within the effective mass approximation, the electron (hole) Hamiltonian of the QD in the applied electric field can be expressed by[46]

$$H_j = \frac{\hbar^2}{2m_{*j}} \nabla_j^2 + V_j(x_j, y_j, z_j) \pm eFz_j \quad (1)$$

where the subscript $j = e(h)$ is the electron (hole), $m_{e*}(m_{h*})$ denotes the effective mass of the electron (hole), and $V_e(V_h)$ represents the confinement potential of the electron (hole). The sign "+" is for the electron while "−" is for the hole. The spectral shift under the electric field is given by[47]

$$\otimes E = \Gamma \sum + \frac{1}{2} \langle \sum^2 + \ldots \quad (2)$$

where E is the energy of the transition, $\sum$ denotes the local field induced by fluctuating surface charges, and μ and $\langle$ represent pro- jections of the excited state dipole moment and polarizability, respectively. To sum up, the electric-field-induced quantum-confined Stark effect has been showed by theory and experiments.[48]

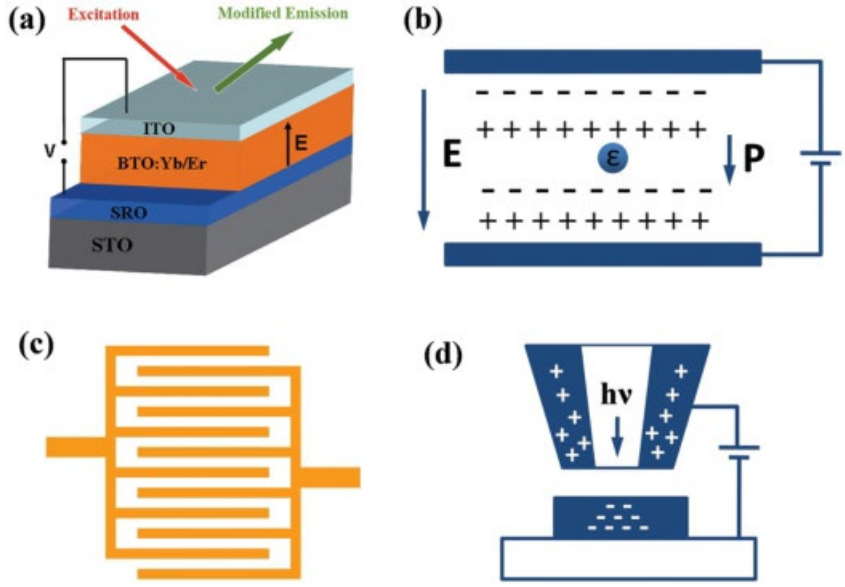

Figure 3. Experimental method and setup of electric-field-induced tuning. a) The setup used for measuring PL of Yb/Er-doped ferroelectric BTO thin films with parallel plate capacitor structure under an electric field. Reproduced with permission.[51] Copyright 2011, John Wiley & Sons, Inc. b) Phosphor composite film with parallel plate capacitor structure under an electric field. c) The patterned metal interdigitated electrodes. d) An electrically biased near-field optical probe.

It should be emphasized that dielectric hosts are commonly used in activator-doped phosphors. When dielectric phosphors are polarized by an external electric field, the electric charges slightly shifted from their average equilibrium positions can cause dielectric polarization. Due to the dielectric polarization, positive charges are shifted toward the field and negative charges displace in the opposite direction. The external electric-field-induced charge distribution leads to a variation of the host symmetry and crystal field around the activator ions. The variation of the host symmetry and crystal field around the activator ions could result in tunable luminescence of metal-ion-doped dielectric phosphors. Taking Ln^{3+}-doped phosphors as an example, electric-field-induced luminescence tuning can be theoretically explained by classical Judd–Ofelt (J–O) theory.[49] According to J–O theory, the theoretical oscillator strength of an electric dipole transition from an initial state $|S, L, J\rangle$ to an excited state $|S2, L2, J2\rangle$ can be written as

$$f_{\text{theor}}^{\text{ED}} = \frac{8\pi^2 m_e \nu}{3h(2J+1)} \frac{(n^2+2)^2}{9n} \sum_{t=2,4,6} \Omega_t \left| \langle S,L,J \| U^t \| S2,L2,J2 \rangle \right|^2 \quad (3)$$

where m_e is the effective mass of electron, h represents Planck's constant, J denotes the total angular momentum for the ground state, ν represents the transition frequency, $\|U^t\|$ is the reduced matrix element which is insensitive to the host environment, and n is the refractive index. Ω_t ($t = 2, 4, 6$) are the J–O intensity parameters. Theoretically, the three parameters Ω_t strongly depend on metal–ligand distances and geometry. Specifically, Ω_2 is more sensitive to changes in symmetry, while the higher rank parameters Ω_4 and Ω_6 are more sensitive to changes in distance.[50] Hence, luminescence tuning can be achieved by the tunable parameter Ω_t induced by coupling the host symmetry around activator ions. Application of electric field could be considered one of the variables capable of varying the symmetry of some specific hosts.

As discussed above, when applying an electric field, the luminescence of phosphors can be tuned due to the Stark effect or dielectric polarization. For measurements under an applied electric field, several experimental methods are proposed. A parallel plate capacitor configuration can be utilized in the modulation of the luminescence of phosphor thin films (**Figure 3**a).[51] Such thin films can be grown on substrates with conductive layers by pulsed laser deposition, molecular beam epitaxy (MBE), and sputtering. Additionally, composite films can be deposited from organic or inorganic compounds by the sol–gel method (Figure 3b).[52] In the measurement, the excitation and emission light beams should pass through the top electrode. Consequently, a transparent electrode of indium tin oxide or another compound is deposited on the top of the phosphor thin film. The small thickness of the phosphor thin film facilitates the application of a sufficiently strong electric field on the phosphor layer under low bias voltages. Also, utilizing photolithographically patterned metal interdigitated electrodes on phosphor films, or placing nanocrystals over the patterned metal interdigitated electrodes, a lateral electric field can be applied to the phosphors (Figure 3c).[53] In addition, spatially localized electric-field-induced tuning of luminescence in nanostructures is presented with an electrically biased near-field optical probe (Figure 3d).[54]

3.2. Magnetic Field-Induced Tuning

Magneto-optic effects have been well documented in the literature. For instance, the Faraday effect expresses variations

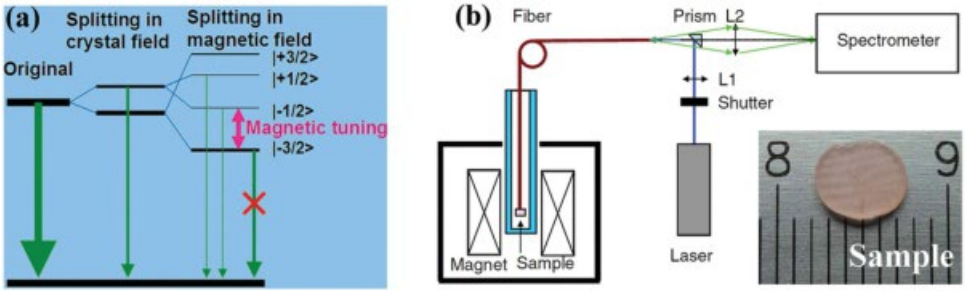

Figure 4. Magnetic-field-induced tuning. a) The Zeeman splitting of energy levels of Er^{3+} ions under an applied magnetic field. Reproduced with permission.[56] Copyright 2013, John Wiley & Sons, Inc. b) A typical experimental setup for measuring the magneto-PL of phosphors. Reproduced with permission.[60] Copyright 2013, Optical Society of America.

in the transmission of light through a magnetic material, and the Kerr effect designates changes to reflected light from a magnetic surface.[55] However, the underlying mechanism for magnetoluminescence has not been fully understood. In fact, magnetic-field-induced luminescence tuning is related to the Zeeman splitting of energy levels upon exposure to magnetic fields. As shown in **Figure 4**a,[56] the tunable luminescence from metal-ion-doped phosphors by a magnetic field can be explained by the $^4S_{3/2}$ and $^4I_{15/2}$ energy levels of Er^{3+} ions under an applied magnetic field. The crystal field exerted on the energy levels by the host leads to the splitting of the original level into two doublets. When a magnetic field is applied on the Er^{3+}-doped phosphor, the two doublets further split into four quartets owing to Zeeman splitting, namely |+3/2>, |□3/2>, |+1/2>, |□1/2>. Then, the separation between |□1/2> and |□3/2> enlarges with increasing magnetic field. The increased separation results in a larger splitting of the |±3/2>
doublet and a negligible radiative probability from |+3/2> to |□3/2>. Meanwhile, most of the emissions originate from the lowest |□3/2> level in the $^4S_{3/2}$ quartet. As a result, the external magnetic field decreases the visible emission intensity from the $^4S_{3/2}$ quartet of Er^{3+} ions.

In theory, the whole physical picture of semiconductors under a magnetic field is complex and there are numerous models to compute and model the magneto-PL phenomena.[57] Moreover, magnetic tuning in semiconductor materials can be observed by using Faraday geometry (magnetic field direction parallel to the growth direction (Z) of materials, $B//Z$) or Voigt geometry (magnetic field direction perpendicular to the growth direction of materials, $B\infty Z$). There is a general trend that the PL emission wavelengths of nanostructured semiconductors shift upon application of a magnetic field.[58] The shifts are due to the diamagnetic shift of excitons.[59] Therefore, a simple proportional relationship between the emission energy shift ($\otimes E$) and the applied magnetic field (B) can be expressed as $\otimes E$ □B_2.

An experimental setup for measuring the magneto-PL of phosphors is shown in Figure 4b.[60] The measuring part consists of a DC-pulsed magnet inside a cryostat cooled by nitrogen gas, and the sample is mounted between the pair of magnet. The laser beam is transmitted through an optical fiber to stimulate luminescence from the phosphor sample. The corresponding magnetic tuning luminescence is collected by the same fiber and recorded by the spectrometer.

3.3. Plasmon-Induced Tuning

In physics, a plasmon, arising from the quantization of plasma oscillations, can be considered a quasiparticle. The existence of plasmons is rooted in the interactions of an incoming electric field with the electrons in a metal nanostructure. Initially, the electric field component of the incoming light induces a polarization among the electrons in the conduction band and the static, positively charged ions. Owing to the displacement of the electrons, a net charge difference is established at the nanoparticle boundaries and therefore creates a linear restoring force to the system.[61] In fact, this created dipolar oscillation of the electron is known as a surface plasmon oscillation. The effect is named with the word "surface" because the main effect producing the restoring force is the surface polarization. The polarization (P) and the incoming electric field (E_0) can be related by the well-known equation[61]

$$P = \langle \sum_m E_0 \tag{4}$$

where ⟨ is obtained from the solution of Laplace's equation, $\sum_m$ represents the dielectric constant of the surrounding medium and static polarizability of the particle. The term "surface plasmon resonance" (SPR) refers to collective oscillations of the surface free electrons at an interface between two matters stimulated by incident light, when the frequency of light photons matches the natural frequency of surface electron oscillations.[62] The underlying physics of SPRs in metallic nanoparticles can be explained by the formulation in Mie's theory. However, it is of vital importance to note that Mie's theory assumed that the particles and their surrounding medium are each homogeneous and depicted by their bulk optical dielectric functions. Considering a nanoparticle with spherical geometry and a radius of R, where $2R \ll$ □, the dielectric function is given by a real and imaginary part[63]

$$\Sigma = \Sigma_1(\square) + i\Sigma_2(\square) = (n + i\square)_2 \tag{5}$$

where n represents the refractive index and | is associated with light absorption. Here, $\sum_m$ is usually derived from a real constant throughout the visible regime and hence it is possible to find a resonance frequency. Equation (5) is then further modified into Equation (6) as

$$[\Sigma_1 \rceil + 2\Sigma_2]^2 + [\Sigma_2 \rceil)]^2 = \text{minimum} \quad (6)$$

in which 'minimum' denotes a minimum value. As a result, the plasma resonance is given by the wavelength dependence of $\Sigma_1(\rceil)$ when the condition of $\Sigma_m = \square 2\Sigma_s$ is fulfilled, and the local field at the particle is enhanced. From the above equations, one should notice that the resonance properties of nanoparticles are dependent on the surrounding environment and the properties of the respective nanoparticles.

It is well known that SPRs play a key role in many areas, such as surface-enhanced Raman spectroscopy, magneto-plasmonics, colour control of materials, and so on.[64] SPR in nanostructures is called localized surface plasmon resonance (LSPR). Metal nanostructures exhibiting LSPR have widely been used to modify excitation or emission rates of nearby emitters, leading to either enhancement or quenching of the luminescence.[65] The LSPR is an effect due to the collective oscillation of electrons on the metal nanoparticles, which may have either beneficial or deleterious effects, depending on the position of the SPR peak and the distance of the luminophore from the metal surface. Interestingly, different nanostructures of such ions can absorb different wavelengths, for instance, Au nanoparticles exhibit only one SPR peak while Au nanorods show SPR absorptions at two peaks.[66]

In general, plasmonic engineering is now routinely performed in luminescence studies on organic molecules, semiconductor nanostructures (QDs, QRs, and QWs), and lanthanide ion-doped nanocrystals.[67] Based on the shape of the metal structure, there are three different interactions: (1) well-defined metal nanoparticles (nanospheres, nanorods, nanodisks, and nanotriangles); (2) a metallic film or surface; and (3) patterned metal nanostructures. Metal nanoparticles can typically be utilized to enhance the fluorescence intensity and decrease the lifetime. Such modifications occur by the strong resonance coupling between the excited nanostructures and localized surface plasmons (LSPs) of the well-defined metal nanoparticles (**Figure 5**a).[68] Controlling the particle's shape and size can modulate the effect of the SPR on the luminescence of phosphors. Highly directional emission can be achieved by utilizing the interactions of photons with thin metallic films (Figure 5b).[69] The thin metallic films are extremely suitable to modulate the luminescence of thin film heterostructures, such as QWs. It is known that a tuning of the uminescence occurs by coupling QDs to metal nanostructures, strongly depending on their shape and distance. Differently shaped metal nanostructures exhibit distinct SPR peaks. By putting QDs closer to the metal nanostructures, the emission of QDs will be enhanced. However, if QDs are too close to the metal, quenching of luminescence will occur. Thus plasmon-controlled fluorescence can be achieved in patterned metal nanostructures by controlling the shape of and distance between the nanostructures (Figure 5c).[65]

3.4. Photon-Assisted Tuning and Ionizing Radiation-Induced Tuning

The photon is a fundamental particle in physics, exhibiting wave–particle duality. Over the past several decades, laser technologies have been widely used to process various materials, particularly using ultrashort lasers with a high resolution in time and space. The electric field strength of a focused ultrashort laser pulse can be up to 100 TW·cm$\square$2, which is sufficient for inducing many nonlinear optical effects in photonic materials, when the pulse energy is 1 μJ and the width is 100 fs. Hence, focused ultrashort-pulse lasers can be employed to induce various microstructural changes in transparent materials.[70] Femtosecond ultrashort pulse lasers have been utilized to fabricate many types of functional optical devices, including photonic crystals, couplers, optical waveguides, and 3D optical storage devices.[71] For instance, using the ultrashort-pulsed light, microscopic modifications of luminescence have been successfully achieved in photonic glasses (**Figure 6**a).[72]

Photoreduction of active ions with ultrashort-pulse lasers is one remarkable way to modulate the luminescence of phosphors. Once the valence state of the activator centre changes, the luminescence of phosphors will be modulated (Figure 6b).[73] Using space-selective irradiation by an ultrashort-pulse laser, simultaneous tuning of the dopant distribution and matrix phase evolution has also been presented in the glassy phase. Using an 800-nm mode-locked pulse laser and an XYZ stage, parallel waveguide structures can be written inside the glass bulk (Figure 6c).[74] With the benefit of the ultrashort pulse duration, the orderly precipitation of nanocrystals Ga_2O_3 and LaF_3 and the selective incorporation of metal ions into them can be achieved.

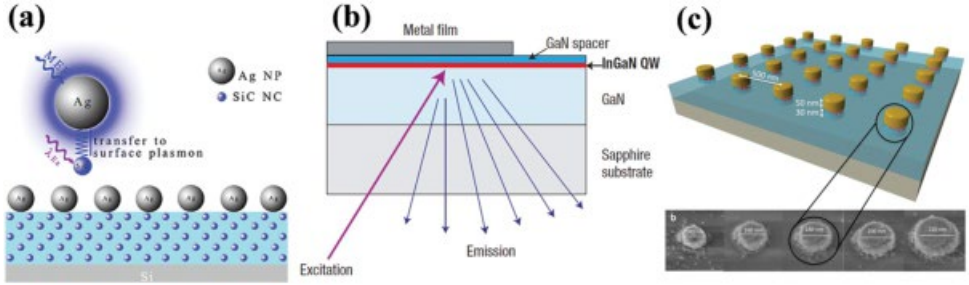

Figure 5. Experimental method and setup of plasmon-induced tuning. a) The PL enhancement system of Ag nanoparticles and SiC nanocrystals in sodium dodecyl sulfate dielectric on a Si wafer. Reproduced with permission.[68] Copyright 2013, IOP Publishing. b) Coupling the thin metallic films with QWs. Reproduced with permission.[69] Copyright 2004, Nature Publishing Group. c) Patterned metal nanostructures. Reproduced with permission.[65] Copyright 2013, Nature Publishing Group.

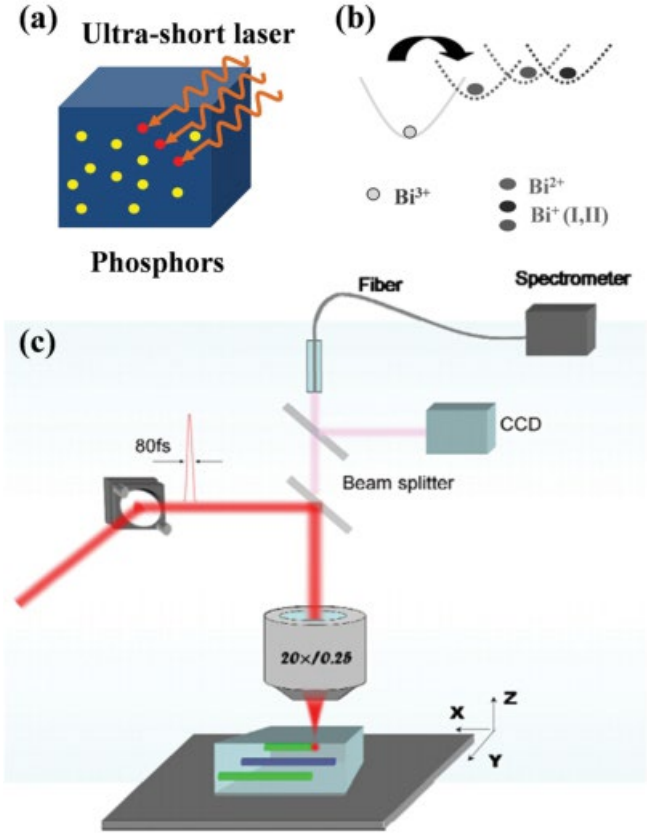

Figure 6. Experimental method and setup of photon-assisted radiation-induced tuning. a) The interaction between phosphors and ultrashort laser pulses. b) The photoreduction reaction of Bi^{3+} ions to Bi^{+} species. Reproduced with permission.[73] Copyright 2009, The Royal Society of Chemistry. c) The setup for space-selective irradiation by an ultrashort-pulse laser. Reproduced with permission.[74] Copyright 2010, American Chemical Society.

In addition, the employment of a filtered light has proven to be a simple and effective method for tuning PL.[75] Through changing the cutoff filter and controlling the illumination time, the emission wavelength can be modulated, owing to self-regulated arrangement of the absorption edge and the Si crystalline size in porous silicon.[76] Moreover, UV irradiation can increase the luminescence quantum efficiency of a nanophosphor coated with polymers, resulting in cured passivating polymers.[77]

Compared to photons, ionizing radiation possesses much higher energy. Ionizing radiation is capable of liberating electrons from atoms or molecules and breaking chemical bonds, thereby ionizing them. Utilizing ionizing radiation with appropriate doses, the luminescence of phosphors can be modified due to the radiation-induced defects or radiation-induced tuning of dopant valence states, or radiation-induced matrix phase evolution.[78] In general, the most common forms of ionizing radiation include ⟨-, ®-, ©-, and X-rays.[79]

3.5. Mechanical Stress-Induced Tuning

In solid mechanics, stress is a fundamental physical quantity that expresses the average force per unit area. Generally, stress in a solid may be due to multiple physical causes, including internal processes and external influences, such as contact forces, external loads, ambient press, ultrasonic vibration, changes in temperature and phase, and electromagnetic fields. The utilization of stress in a solid possibly changes its physical properties, including polarization, birefringence, permeability, and luminescence. Stress also usually creates some strain in the solid and leads to structural or chemical modifications. The structural modifications are connected with the energy levels or the bandgap, and the chemical changes are associated with the physical properties. Recently, Wang developed a new research field of piezo-phototronics.[80] The piezo-phototronics effect is a three-way coupling among piezoelectricity, luminescence, and semiconductor behavior. It suggests that applying strain to a semiconductor with piezoelectricity can tune the charge transport behavior and then improve the performance of optoelectronic devices.[81]

In general, various mechanical stimuli, which are often encountered in research and engineering designs, include friction, impact, compression, and ultrasonic vibration. Utilizing the desired stress, tuning of the luminescence of phosphors can be achieved. It is noteworthy that one kind of phosphor is sensitive to stress, namely elastico-mechanoluminescent (EML) materials. EML materials can convert various local mechanical energies into light emission. By dispersing the EML particles into an optical polymer, a multiple stress-sensitive hybrid film can be fabricated. Then luminescence of the prepared hybrid phosphor film can be investigated under various external stimuli (**Figure 7**a).[82] Furthermore, through tailoring the substrate-induced strain of thin film heterostructures, the luminescence properties of phosphors can be finely tuned. Among many types of substrates, $Pb(Mg_{1/3}Nb_{2/3})_{0.7}Ti_{0.3}O_3$ (PMN-PT) is capable of providing large biaxial strain arising from converse piezoelectric effects, due to its large piezoelectric coefficients ($d_{33} > 2000$ *p*C/N) and high electromechanical coupling factors ($k_{33} > 0.9$). The developed method of electric-field-controlled strain has previously been applied to modulate transport,[83] magnetic,[84] and optical[85] behaviors of different material systems. Benefiting from piezoelectric-induced strain of PMN-PT, the luminescence of phosphors can be modulated in a real-time and reversible way on the basis of on-wafer devices. Very recently, with this controllable piezoelectric-induced strain from PMN-PT, some groups have successfully tuned the luminescence of QD in *p-i-e* LEDs (Figure 7b),[86] and metal-ion-doped thin film phosphor samples[87] (Figure 7c). Through strain engineering, the band edges of semiconductor nanostructures are modulated by bending the samples with stages (Figure 7d, e).[88] Such uniaxial stress can also be used to modify the structure, e.g., Schottky barrier, leading to the tuning luminescence of the device (Figure 7f[89]).

Besides stress-induced luminescence tuning, ultrasound-induced gelation of some organic liquids can also be performed to tune the luminescence. Ultrasound control of the aggregate morphology results in an observed change in the luminescence.[90]

3.6. Temperature-Induced Tuning

Microscopically, the lattice vibration quantized as a phonon is associated with temperature and the lattice waves.[91]

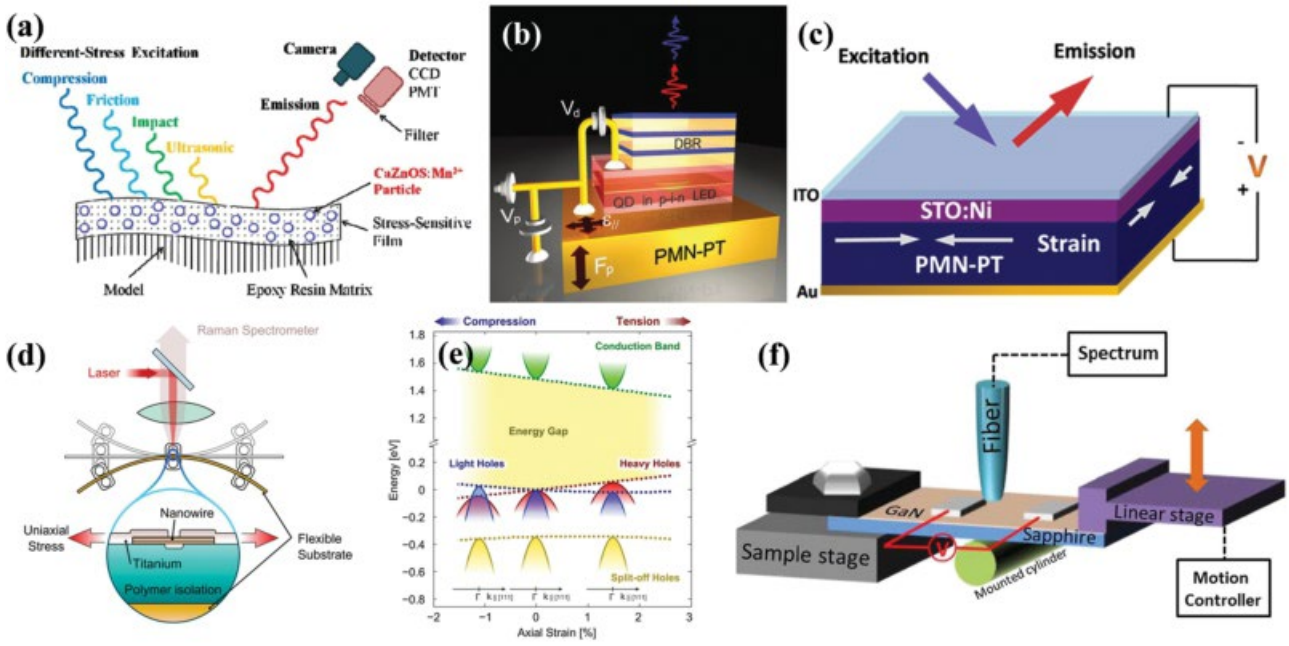

Figure 7. Experimental method and setup of stress-induced tuning. a) The setup used for measuring various ML. Reproduced with permission.[82] Copyright 2013, Optical Society of America. b) A *p-i-n* nanomembrane containing QDs is integrated on top of a piezoelectric actuator (PMN-PT). Reproduced with permission.[86] Copyright 2012, John Wiley & Sons, Inc. c) The setup used for measuring the emission of STO:Ni/PMN-PT under the piezoelectric-induced strain induced by an external electric field. Reproduced with permission.[87] Copyright 2014, Nature Publishing Group. d) Schematics of the bending principle illustrating stress effects on individual nanowire structures. e) Expected shift of the band edges of GaAs nanowires under uniaxial stress. Reproduced with permission.[88] Copyright 2013, American Chemical Society. f) The setup for bending a thin film luminescent device sample. Reproduced with permission.[89] Copyright 2012, American Chemical Society.

Previous studies have reported that the change in luminescence upon increasing temperature was related to a higher multiphonon relaxation rate. As a result, temperature can tune luminescence in metal ion-doped materials mediated by phonons.

It is noted that some commonly used activator ions, such as Ln ions, consist of close energy levels, such as the $^2H_{11/2}$ and $^4S_{3/2}$ energy levels of Er^{3+} ions and $^3F_{2,3}$ and $^3H_4$ of Tm^{3+} ions. In particular, the doublet of $^4F_{3/2}$ energy levels of Nd^{3+} ions is only separated by about 60 cm□.[92] Thanks to the small energy separation, the energy transitions are readily susceptible to thermal agitation. In addition, the relative PL intensities related to those close energy levels are governed by the Boltzmann law (Equations (7) and (8)) and Er^{3+} ions are used as an example as follows:[93]

$$\frac{I_{525}}{I_{545}} = Ce^{\frac{\square\otimes E}{KT}} \tag{7}$$

$$C = \frac{\text{™}_H \rceil_H g_H}{\text{™}_S \rceil_S g_S} \tag{8}$$

where I_{525} and I_{545} are the luminescence intensities of $^2H_{11/2}/^4S_{3/2}$ □$^4I_{15/2}$ transitions, C is a constant depending on ™, ⌉, and g; ™, and ⌉correspond to the emission cross section and angular frequency of the $^2H_{11/2}/^4S_{3/2}$□$^4I_{15/2}$ transitions, respectively. g_H and g_S are the degeneracies of level $^2H_{11/2}$ and $^4S_{3/2}$, respectively. ⊗E is the energy gap between the two states.

In addition to the relative change in the intensity of emission wavelengths, the overall emission intensity also changes with temperature. The underlying reason for this overall intensity change is the electron–phonon interaction at various temperatures. Thus, the intensity I_i of luminescence can be written as

$$I_i = N_i R_i \mid = N_i(T) R_i \mid \tag{9}$$

where $N_i(T)$ denotes the population of the excited states at the temperature T, R_i is the radiative rate, and ⏐ is the lifetime of the excited states.[94] ⏐ depends on the radiative rate R and nonradiative transition rate W_{NR}, which can be expressed as[95]

$$\frac{1}{\mid} = + _{NR} \tag{10}$$

It is also known that the nonradiative transition rate of multiphonon relaxation in the Ln^{3+} ions can be expressed as

$$W_{NR}(T) = W_{NR}(0)[1 \square \exp(\square\rceil / k_B T)]\square^p \tag{11}$$

where $W_{NR}(0)$ is the nonradiative rate at zero temperature, ⌉ is the phonon energy, p is the number of phonons involved.[96]

By substituting Equation (9) to Equation (11), the emission intensity is explicitly given by

$$I_i = N_i \square exp[\square p_i \otimes E / k_B T)][\exp(\square k_B T / E_q)]^{pi} \{1 \square W_{NR}(0)[1 \square \exp(\square\rceil / k_B T)]\square^p\} \tag{12}$$

From Equation (12), it should be noted that the □temperature-dependent luminescence intensity is governed by competing processes between the thermal agitation and nonradiative decay. Therefore, in the low temperature range, the thermal distribution rate is high while the nonradiative rate is very low, which results in the increase of emission intensity as temperature increases. However, the nonradiative rate increases rapidly at high temperatures and causes the radiation probability to decrease significantly. Therefore, the emission intensity decreases in the high temperature range.

Apart from metal ion-doped phosphors, temperature can also affect the luminescence in semiconductors. Previous reports have indicated that the luminescence intensities, bandwidth, and emission wavelengths change abruptly with temperature in various types of structures, such as thin films, nanobelts, nanowires, and QDs.[97] The decrease in luminescence intensity upon increasing temperature can be explained by thermally activated carrier trapping and nonradiative recombination at defect sites.[98] The redshifting of emission wavelength can be revealed by the Varshni relation (Equation (9)),[99] which was previously used to describe the temperature dependence of the bandgap (E_g) in bulk semiconductors. The validity has been proven by Chin et al.[100]

$$E_g = E_0 - \alpha T^2/(T + \beta) \tag{13}$$

where R is the temperature coefficient, ® is approximately the Debye temperature of the material, and E_0 is the bandgap at 0 K. This equation implies that the bandgap of a semiconductor is sensitive to temperature change and therefore the emission shift. Moreover, the emission peaks show broadening upon increasing temperature, and Valerini et al. attributed the broadening to carrier-phonon scattering processes. To shed more light on this effect, Equation (10) can be used to describe temperature dependence of the excitonic peak broadening in QDs,[101]

$$\Gamma(T) = \Gamma_{inh} + \gamma T + \Gamma_{LO}\left(e^{E_{LO}/kT} - 1\right)^{-1} \tag{14}$$

where Γ_{inh} is the inhomogeneous broadening, independent of temperature, and it is due to fluctuations in the size, shape, and composition of the nanocrystals. The last two terms represent the homogeneous broadening as a result of exciton–phonon interactions, γ is the exciton–acoustic phonon coupling coef- ficient, Γ_{LO} represents the exciton–longitudinal-optical (LO) phonon coupling coefficient, E_{LO} is the LO-phonon energy, and k is the Boltzmann constant.

Meanwhile, temperature also affects the emission intensity and shifts the emission wavelength in organic polymers and molecules. The emission intensity of organic phosphors is governed by the following equation:[102]

$$I_{0\to n} = \frac{e^{-S} S^n}{n!} \tag{15}$$

where I is the corresponding transition intensity from the 0th vibronic-excited state to the nth vibronic ground state, S is the Huang–Rhys factor and it is temperature dependent. $S = M\omega/2\hbar\otimes^2$,[103] ω is the vibrational frequency, M is the reduced mass of the harmonic oscillator that couples to the electronic transition, and ⊗ is the displacement of the potential curve between the ground and excited states. Therefore, S describes the average number of phonons that are involved when the excited molecule relaxes from its ground state configuration to the new equilibrium configuration in the excited state. Assuming that ω is the same for ground, excited states and that the potentials are perfectly parabolic, the transition matrix elements are the same for all vibronics and neglect all vibronics above 0–3, S can be simply found by calculating the fractional intensity of the vibronic peaks, as shown in Equation (16):

$$S = \left(I_{0\to1} + 2I_{0\to2} + 3I_{0\to3}\right)/I_{total} \tag{16}$$

On the other hand, the redshift and blueshift of the emission wavelength depend on whether the organic material is a long-chain polymer or a conjugated molecule. Conjugated polymers tend to show blueshifting of their PL transition energies with increasing temperature, independent of their actual backbone conformation. The shifts in the emission wavelengths reflect the temperature dependence of the actual relaxation process whereby the exciton remains more localized on smaller chain segments with increasing temperature. However, short conjugated molecules behave like bulk semiconductors, where the redshift of the emission wavelengths increases with increasing temperature, indicating a renormalization of band energies due to electron–phonon interactions. Therefore, the shifts can also be described by Bose–Einstein statistical factors for phonon emission and absorption, as shown in Equation (17),

$$E_g = E_0 - 2a/[\exp(\theta/T) - 1] \tag{17}$$

where E_0 is the bandgap energy at 0 K, and a is the strength of the exciton–phonon interaction. This includes the contribution from both acoustical and optical phonons. θ is the average phonon temperature.[104]

Based on the above-introduced principles of tuning luminescence using physical methods, we next review some research advances of tunable luminescence in various types of phosphors, including metal ion-doped phosphors, nanostructured semiconductors, and stimuli-responsive organic phosphors.

4. Metal Ion-Doped Phosphors

To date, numerous kinds of metal ion-doped phosphors have been fabricated in different forms such as glass bulk,[105] crystal bulk,[106] powders,[107] nanoparticles,[108] and thin films,[109] in which the luminescence properties mainly depend on the energy transition of activators in the phosphors. Generally, three types of metal ions usually serve as impurities, i.e., lanthanide ions, transition metal ions, and main group metal ions. The luminescence of metal ion-doped phosphors can cover a broad optical spectral range, including UV, visible, and infrared regions. In particular, metal ion-doped phosphors have drawn great attention due to their widespread application from optoelectronics to biomedicine, through to approximately every aspect of human life.

4.1. Lanthanide Ion-Doped Phosphors

The lanthanide series of chemical elements comprise 15 metallic elements, from lanthanum (atomic number 57) to lutetium (atomic number 71). Besides La^{3+} being equivalent to Xe in electronic configuration, the lanthanide ions (Ln^{3+}) have one to fourteen 4f electrons added to their inner shell configuration from Ce^{3+} to Lu^{3+}.[110] Apart from La^{3+} and Lu^{3+}, due to the partially filled 4f shell, the Ln ions have abundant ladder-like energy levels and exhibit a variety of luminescence properties in the UV, visible, and NIR regions.[111] Therefore, Ln ions are widely used as luminescent ions in phosphors.[112]

4.1.1. Electric Field-Induced Tuning

Our group has reported electric field-mediated upconversion PL tuning of a ferroelectric $BaTiO_3$ (BTO):Yb/Er thin film in a heterostructure device.[51] The device consists of a BTO:Yb/Er film deposited on conductive $SrRuO_3$ (SRO)-coated $SrTiO_3$ (STO) substrates. As a result, the NIR excitation can be absorbed by the Ln^{3+}-doped BTO film to generate upconverted emission. Due to the hypersensitive green band emission ($^2H_{11/2}/^4S_{3/2} \rightarrow {}^4I_{15/2}$) of Er^{3+} ions, the overall green band emission intensity was enhanced 2.7 times under a voltage of 10 V while the intensity of the red emission ($^4F_{9/2} \rightarrow {}^4I_{15/2}$) of Er^{3+} ions had little change (**Figure 8**a). According to Equation (3) shown in Section 3, the difference in the enhancement factors of green and red emission bands is due to the fact that the local symmetry influence on the corresponding intra-4f transitions varies greatly. Consequently, a tunable green-to-red ratio was found under different biasing voltages on the device. Importantly, the unique structure of ferroelectrics provides us with the opportunity to realize emission tuning in a reversible and dynamical manner.

In addition, other research groups have observed that electric poling can affect the luminescence of ferroelectric ceramics. For instance, through poling of ferroelectric $Bi_{0.5}Na_{0.5}TiO_3$: Pr^{3+} ceramic, an enhanced PL has been observed due to the decrease in the crystal symmetry around Pr^{3+} ions.[113] Meanwhile, PL quenching of Pr^{3+} ions was obtained in $(Ba_{0.7}Ca_{0.3}TiO_3)$-$(BaZr_{0.2}Ti_{0.8}O_3)$:Pr^{3+} ceramics after polarization.[114] The reason was deduced to be the electric ield-induced structural phase change from rhombohedral to tetragonal.

4.1.2. Magnetic Field-Induced Tuning

An early work on magnetic tuning was reported by Tikhomirov et al.,[115] in which the emission intensity decreased in PbF_2:Er nanoparticles by two orders of magnitude under a magnetic field of up to 50 T. Later on, Singh et al.[116] observed magnetic-induced bistability in Gd_2O_3:Yb/Er nanoparticles. An eight-fold decrease of PL intensity was observed under a magnetic field of 1 T. Moreover, they showed that the integrity of the emission can be retained by cycling the Gd_2O_3:Yb/Er from 0 to 1 T (Figure 8b). Recently, a detailed study of the magnetic tuning effect has been reported based on $NaGdF_4$:Nd/Yb/Er nanoparticles.[56] The emission intensity was tuned down to 60% and

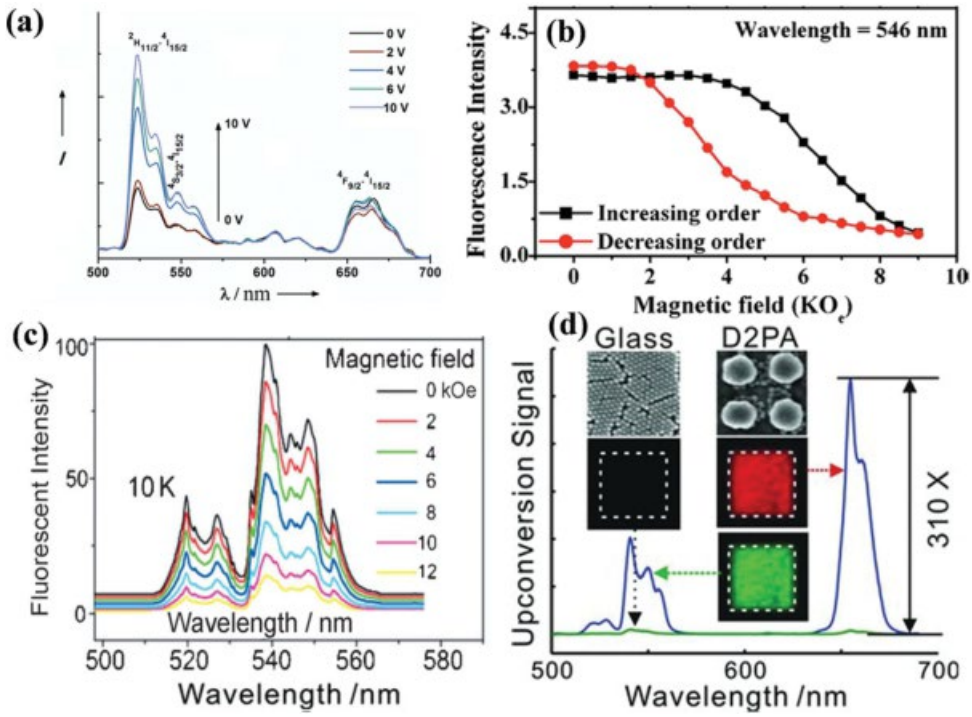

Figure 8. Tuning the luminescence of lanthanide ion-doped phosphors. a) The emission spectra of the BTO:Yb/Er film under an electric field. Reproduced with permission.[51] Copyright 2011, John Wiley & Sons, Inc. b) The emission intensity at 546 nm of the Gd_2O_3:Yb/Er nanoparticles under an external magnetic field from 0 to 1 T. Reproduced with permission.[116] Copyright 2010, Optical Society of America. c) The emission spectra of $NaGdF_4$:Nd/Yb/Er nanoparticles under an applied magnetic field. Reproduced with permission.[56] Copyright 2013, John Wiley & Sons, Inc. d) The PL spectra on D2PA and glass substrates. Reproduced with permission.[121] Copyright 2012, John Wiley & Sons, Inc.

15% of its original intensity at 300 and 10 K under a 12 kOe magnetic field, respectively (Figure 8c). Coordinating magnetic ions (e.g., Gd^{3+}) seem to be necessary in order to observe efficient magnetoluminescence, which is supported by comparing the PL intensity with $NaYF_4$:/Nd/Yb/Er nanoparticles under identical experimental conditions.

4.1.3. Plasmon-Induced Tuning

Schietinger et al. reported plasmon-enhanced luminescence in single $NaYF_4$:Yb/Er nanoparticles.[117] The phosphor nanoparticles and Au nanoparticles are investigated and assembled in a combined confocal and atomic force microscope setup. An overall emission enhancement of 3.8-fold was recorded. Zhang et al.[118] observed enhanced emission by attaching Au nanoparticles onto the surface of poly(acrylic acid) (PAA)- and poly(allylamine hydrochloride) (PAH)-capped $NaYF_4$:Yb/Tm nanoparticles. The emission intensity was amplified by a factor of 2.6 with the attachment of these single Au nanoparticles, however, the subsequent growth of a Au nanoshell suppressed emission as a result of the reduced effective excitation flux. In addition to Au, the presence of Ag nanoparticles is also capable of enhancing emission in a $NaYF_4$:Yb/Er@SiO_2@Ag core/shell nanocomposite.[119] The luminescence enhancement factors of 14.4 and 10.8 were recorded in the presence of 15 nm and 30 nm Ag nanoparticles in the shell, respectively. Saboktakin et al.[120] prepared two types of multilayers of Au and Ag nanoparticles separated by a nanoscale aluminium oxide (Al_2O_3) layer for an SPR emission enhancement study in $NaYF_4$:Yb/Er (Tm) nanoparticles. They found that the enhancement was highly dependent on the thickness of the Al_2O_3 layer. The optimal separations for Au and Ag were 5 and 10 nm, respectively. They further showed that the optimal luminescence enhancement factors of Au were 5.2 and 3.5 at 540 and 650 nm, respectively. Comparatively, the factors for Ag were 30 and 45 at the same emission wavelengths. Recently, with a disk-coupled dots-on-pillar antenna array (D2PA), the enhancement factor of upconversion emission intensity of $NaYF_4$:Yb/Er can reach up to 310 (Figure 8d), meanwhile, the luminescence decay becomes eight times faster.[121] The experimental results and numerical simulations suggest that the large enhancement factor arises when the resonance frequency of the D2PA structure matches the excitation laser's frequency.

4.1.4. Photon-Assisted Tuning and Ionizing Radiation-Induced Tuning

In general, optical excitation is widely regarded as the excitation source for the observation of PL. Furthermore, the bombardment by short-pulsed lasers can cause photoactivated chemical reactions. It is known that some divalent Ln ions (e.g., Eu^{2+}) are unstable in an oxidizing atmosphere. Annealing these phosphors at relative high temperatures for hours in a reducing atmosphere is normally required for the reduction of Eu^{3+} to Eu^{2+}, unless the host has no specific structure groups.[122] In contrast, some Ln^{3+} ions, such as Eu^{3+} and Sm^{3+} ions, can be reduced to their divalent counterparts in ambient conditions with the aid of a photon-assisted technique. The mechanism is due to the charge transfer (CT) states in the deep UV regime, and these CT states are photochemically active.[123] After reduction, the PL property of these ions shows substantial changes. In early studies, Eu^{3+} and Sm^{3+} ions were found to be reduced to Eu^{2+} and Sm^{2+} ions by a nanosecond excimer laser.[124] The reduction processes were achieved by a one-photon absorption process. Further to the photoreduction study in Eu^{3+} ions, the results indicated that shorter wavelengths and using methanol as a medium could enhance the reduction yield of Eu^{2+} ions.[125] On account of advances in laser technology, pico/femto-second-pulsed lasers are readily available. Nobuaki et al. harvested Eu^{2+} from Eu^{3+} ions in methanol by using a picosecond Ti:Sapphire laser operating at 394 nm.[126] The excitation wavelength can match with the transition $^7F_0$□$^5L_6$ and hence the electrons in Eu^{3+} ions can be effectively excited to the CT states for the reduction. The concentration of Eu^{2+} ions increased with each pulse and eventually leveled off. Upon the formation of Eu^{2+} ions, the PL colour of the solution changed from pink to white, accounted for by the mixture of pink colour from the PL of Eu^{3+} and the blue colour from Eu^{2+} ions. A multiphoton ionization process can also be used to perform photoreduction.[127] For example, Nishida et al. adopted a similar method to reduce Eu^{3+} to Eu^{2+} ions by using pulsed fs laser at 800 nm.[128] As shown in **Figure 9**a, the blue PL of Eu^{2+} increased along with the decreasing PL of Eu^{3+}, and this effect was more pronounced at higher pulse energies.

Moreover, external sources beyond the UV, visible, and infrared regimes, such as X-rays[129] and ©-rays,[130] have previously been considered for tuning the PL of Ln^{3+} ions. Huang et al. reported the reduction of Sm^{3+} to Sm^{2+} ions by using X-ray irradiation on Sm-doped $BaBPO_5$ (Figure 9b).[131] In their experiments, the thermal stability of the reduced Sm^{2+} ions was examined by exposing the sample at various temperatures. The reduced sample was able to remain stable up to a temperature of 450 °C. Meanwhile, the effect of © radiation on the PL, absorption, and decay characteristics of Y_2O_3:Eu^{3+} and $SrAl_2O_4$:Eu^{2+} phosphors has been illustrated.[132] Interestingly, the PL spectra and decay characteristics of Y_2O_3:Eu^{3+} phosphor remained intact after irradiation with ©-ray (595 kGy). This result indicates the absence of a reduction of Eu^{3+} to Eu^{2+} in the sample, because the reduction process is a host-sensitive process. In addition, the $SrAl_2O_4$:Eu^{2+} phosphor showed a slight decrease in PL intensity after ©-ray irradiation. The reduction in PL was the consequence of ©-ray-induced defects, which could favor extra nonradiative relaxation.

4.1.5. Mechanical Stress-Induced Tuning

In addition to the above techniques, the application of pressure is another common method to tune the emission from Ln^{3+}-doped phosphors. Valiente et al.[133] reported the redshifting of overall upconversion emission of $KY(WO_4)_2$:Yb/Er phosphors upon increasing the pressure from 0.69 to 7.08 GPa. Güdel and co-workers[134] explored the origin of the high green luminescence efficiency in ®-$NaYF_4$:Yb/Er phosphors. In their experiments, pressure-dependent emission spectra ranging from 0 to 29.7 GPa were recorded at 15 and 300 K. They observed a

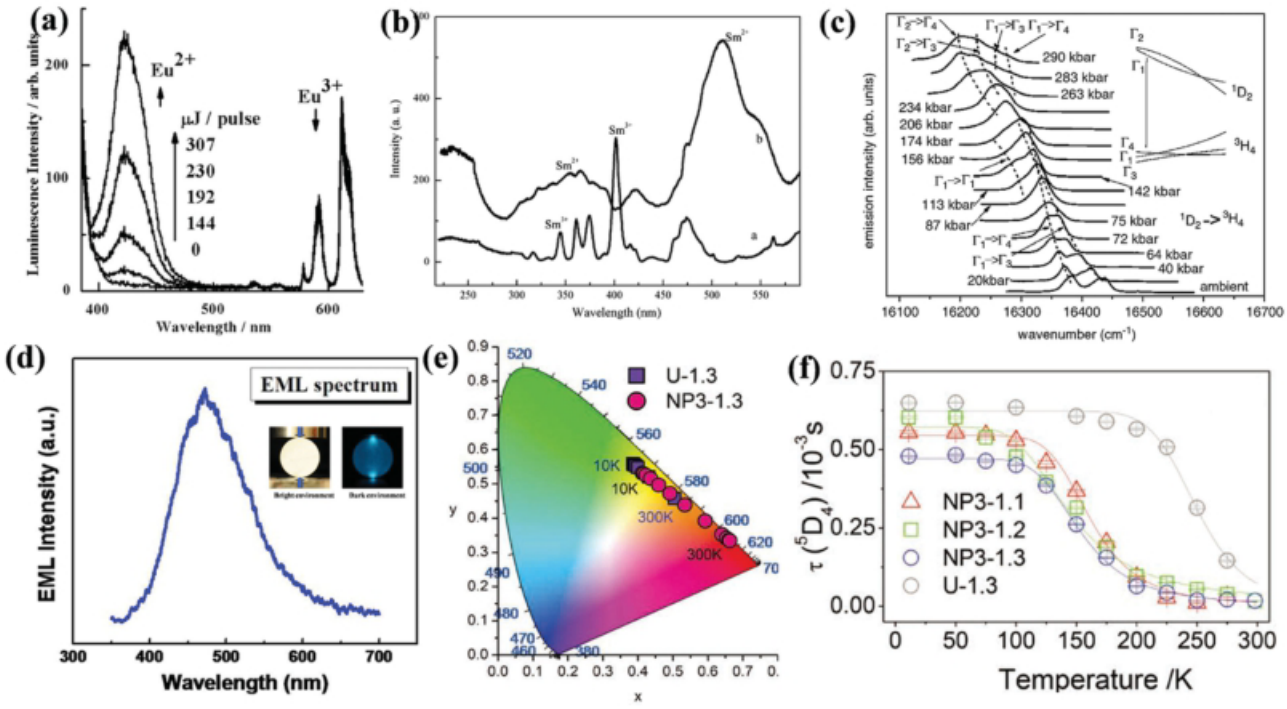

Figure 9. Tuning the luminescence of lanthanide ion-doped phosphors. a) The emission spectra of Eu-doped phosphors irradiated by a pulsed laser with various energies. Reproduced with permission.[128] Copyright 2008, Elsevier B.V. b) The emission spectra of Sm-doped phosphors. a: before © ray irradiation; b: after © ray irradiation. Reproduced with permission.[131] Copyright 2008, Elsevier B.V. c) Pressure-dependent emission spectra of the transition $^1D_2$□$^3H_4$ in YAG:Pr^{3+}. Reproduced with permission.[136] Copyright 2007, Elsevier B.V. d) The ML spectrum of an EML sample under load. The inset shows EML photographs in bright and dark environments, Reproduced with permission.[138] Copyright 2013, Optical Society of America. e) The temperature-dependent colour coordinates (x, y) of Eu/Tb-co-doped hybrid film using Eu:Tb = 1:3 (U-1.3) and Eu/Tb-co-doped nanoparticles using Eu:Tb = 1:3 (NP3–1.3) in the CIE diagram. f) Tb^{3+}:$^5D_4$ lifetime of Eu/Tb-co-doped samples at different temperature. Reproduced with permission.[141] Copyright 2010, John Wiley & Sons, Inc.

reduction in luminescence intensity, which was attributed to pressure-induced detuning between the resonant levels of the Er^{3+} ($^4I_{11/2}$) and the Yb^{3+} ($^2F_{7/2}$). The change in the green-to-red ratio was caused by the reduction of the energy gap between the $^4S_{3/2}$□$^4I_{15/2}$ and $^2H_{11/2}$□$^4I_{15/2}$ transitions upon compression, indicating that high-pressure effects may slightly modify the electron repulsion and spin–orbit interactions responsible for the decrease of the multiplet–multiplet separation. Moreover, pressure can increase crystal-field splitting of the Stark levels in the ground state ($^4I_{15/2}$) and excited state ($^4S_{3/2}$).

Regarding downconverting phosphors, Bungenstock et al. reported a study on the energy-level scheme in Pr^{3+}-doped LaOCl under pressure in the spectral range from 11 000 to 22 000 cm□.[135] Notably, 46 spectral lines of Pr^{3+} were observed under ambient pressure and these lines showed a redshift at a pressure of 16 GPa. To reveal the underlying physics, the free-ion and crystal-field parameters were used to describe the energy-level scheme. The pressure-tuned PL emission was attributed to the change in crystal field strength. Using the same Ln^{3+} ion, Matysiak et al. selected two spectral transitions, $^3P_0$□$^3H_4$ and $^1D_2$□$^3H_4$, in Pr^{3+} doped $Y_3Al_5O_{12}$ (YAG) to study the pressure dependence from ambient to 290 kbar pressure.[136] Figure 9c indicates that all pressure results in redshifts, which are smaller for the lines of lower energies for the emission from the $^3P_0$ and $^1D_2$ states. Also, the ℘1□℘3 and ℘1□℘4 transitions presented different dependencies on pressure. Similarly, they attempted to investigate the pressure-tuning effect by using a superposition model to analyze the crystal field change. The results are contrary to their expectation that the dependence of pressure would be nonisotropic.

It is worth pointing out that the emission of ML materials may respond to various stresses. Particularly, EML materials exhibit an accurate linearity of light emission intensity against stress in the elastic region, which is useful for fabricating stress-optical sensors. Up to now, several Ln^{3+}-doped phosphors, including (Ba, Ca)TiO_3:Pr^{3+} (red), $Sr_3Sn_2O_7$:Sm^{3+} (reddish-orange), $SrAl_2O_4$:Eu^{2+} (green), and $BaSi_2O_2N_2$:Eu^{2+} (bluish-green), have been found to have an intense EML property.[137] For instance, the composite pellet of $CaZr(PO_4)_2$:Eu^{2+} powders/epoxy resin emits a bright cyan emission under a compressive load (Figure 9d).[138] More importantly, the EML composite presents a finely linear relationship between the compressive load and luminescence intensity, when the force is above the load threshold (only 4.86 N). The linear dependence is extremely important for simultaneously sensing and imaging the stress intensity and distribution. The emission peak is due to the transition of Eu^{2+} ions between the excited state $4f^65d^1$ and the ground state $4f^6$. The observed EML phenomena might be attributed to the piezoelectric crystal structure of the hosts and the multiple trap levels with appropriate depths.

4.1.6. Temperature-Induced Tuning

Apart from the above-mentioned physical quantities, temperature also plays an important role in luminescence tuning. Pires et al. reported a temperature-dependent luminescence study on a nanosized Y_2O_3:Yb/Er phosphor from 10 to 300 K.[139] In their work, the upconversion emission (violet, green, and red) and downconversion (NIR) emissions of Er^{3+} ions showed a decrease in luminescence intensity upon increasing temperature. Considering Equation (11) in Section 3, the decrease in luminescence is ascribed to the predominance of multiphonon de-excitation. Hence, the violet emission intensity showed a greater decrease compared to other recorded wavelengths. Interestingly, Gouveia-Neto et al.[140] found that the intensity ratio of upconversion emission at the wavelength 530 and 555 nm in Yb/Er-co-doped chalcogenide glass increased linearly with temperature, increasing from 20 to 225 °C. This finding indicates that Yb/Er-co-doped chalcogenide glass could be used as a thermometer.

Through controlling the temperature of Ln ion-doped compounds, the luminescence of the nanostructured phosphor can be finely modulated, denoted luminescent thermometry.[93a] Interestingly, Carlos's group observed temperature-dependent luminescence properties of Eu/Tb-co-doped ©-Fe_2O_3@TEOS/APTES nanoparticles and a hybrid sensing film.[141] Thanks to the temperature-dependent radiative transition and energy transfer of Ln ions, the emission colour could be finely tuned by changing the temperature (Figure 9e). Figure 9f presents the Tb^{3+}:$^5D_4$ lifetime of the prepared samples at different temperatures. The temperature-dependent lifetime is strongly associated with the thermally activated nonradiative process. Moreover, magnetic field-induced[142] and plasmon-induced[143] temperature increases in Er^{3+}-doped luminescent nanoparticles and films has been found, suggesting that Ln ion-doped nanostructured phosphors are fascinating luminescent thermometers on the nanoscale.

4.2. Transition Metal-Ion-Doped Phosphors

Besides lanthanide ions, mostly transition metal ions are used as activators.[144] In general, transition metal ions have an incompletely filled d-shell.[145] Because of the larger spatial extension of the spectroscopically active d electrons, the energy-level structures of transition metal ions are sensitive to their coordination environment. In general, environmental perturbations, including chemical or structural modifications, can lead to the changing of bond lengths, bond angles, covalence, and coordination number. Hence, the variation in energy-level structure induced by environmental perturbations is usually believed to be responsible for the observed tunable luminescence properties of transition metal ion-doped phosphors.

4.2.1. Photon-Assisted Tuning

The compound ZnS:Mn^{2+} is one of the most important phosphors in EL devices. Through UV irradiation of nanocrystalline ZnS:Mn^{2+} coated with different polymers, including PVB, PMMA, PVA, and MA, a remarkable enhancement in its luminescence was found.[146] The enhanced luminescence is attributed to UV-induced cross-linking, leading to a better passivating polymer coating.[147] Park's group[148] examined the UV irradiation effects on the luminescence properties of ZnS:Mn^{2+} nanoparticles by controlling the irradiation time with oxygen bubbling. As shown in **Figure 10**a, the orange emission around 580 nm is a consequence of the transition of Mn^{2+} ions. The PL intensity enhances constantly with increasing UV irradiation time up to 12 h. At the same time, the quantum efficiency is continuously improved from 16% to 35%. The reason for the significant improvement in the PL properties is that the UV-irradiated surface passivating layer suppresses nonradiative recombination.

4.2.2. Mechanical Stress-Induced Tuning

Utilizing an external continuous pressure, the change in sharp-line luminescence in ruby samples (0.05% wt Cr^{3+}) was measured by Block et al.[149] A small fragment of a ruby crystal was placed in the diamond pressure cell with the studied substances. The tuning of ruby sharp-line luminescence under pressure is apparent (Figure 10b). The *R*-lines originate from the electronic transitions between the ^2E and $^4A_2$ crystal field split states of the Cr^{3+} ion. The ^2E level is converted into two splitting levels, which is responsible for the two emission peaks (R_1 and R_2). With increasing the pressure, the *R*-line luminescence shows a redshift, the emission intensity gradually decreases, and the linewidth broadens. The line shift is linearly proportional to the applied pressure (□0.77 ± 0.03 cm□ kbar□ for R_1 and □0.84 ± 0.03 cm□ kbar□ for R_2), indicating that a pressure measurement can be made by the utilization of *R*-line luminescence. Under external pressure, the ^2E level is compressive, which causes the red line shift.

Similarly, Wenger et al. investigated the luminescence properties of 3d-metal systems (NaCl:Ti^{2+} and $CsCdCl_3$:Ni^{2+}) under an external hydrostatic pressure. The pressure-dependent luminescence spectra of NaCl:Ti^{2+} at 15 K under 15454 cm□ excitation were reported.[150] Each spectrum includes two broad emission bands: one located in the visible area and another one located in the NIR range. With increasing pressure, both bands shift to higher energies due to pressure-induced changes in force constants and equilibrium distortions of the emission electronic states $^3T_{2g}$ and $^3T_{1g}$. Compared to the above Ln ion-doped phosphors, the pressure-induced emission shift is more remarkable in transition metal ion-doped phosphors. The difference in the tuning luminescence between the two kinds of phosphors is understandable when considering the fact that the energy levels of transition metal ions are more sensitive to the surrounding environment.[17]

Based on the piezo-phototronic effect, dual-mode light and ultrasonic emissions have been presented in ZnS:Mn/PMN-PT thin film structures by our group.[151] Apart from the generation of emission, tuning of the luminescence originating from the transition metal ion Mn can also be realized via biaxial strain controlled by an applied voltage upon a piezoelectric PMN-PT crystal. Under an AC electric field, ZnS:Mn gives an orange emission with a peak at 588 nm. Figure 10c

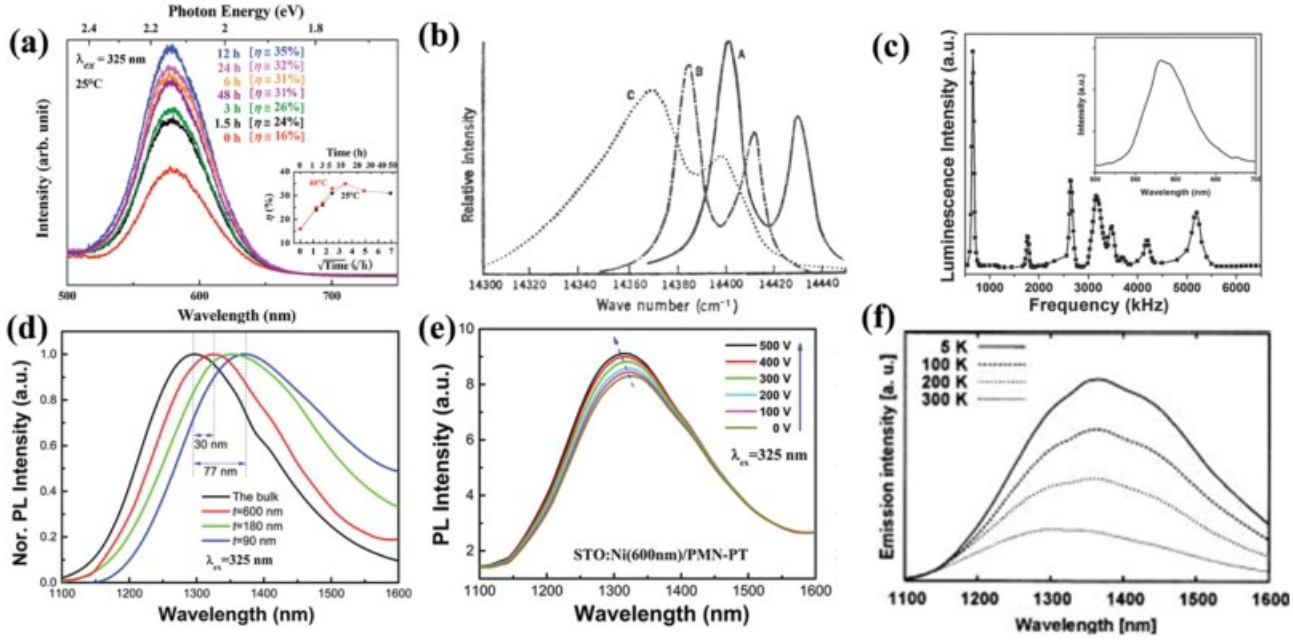

Figure 10. Tuning the luminescence of transition metal ion-doped phosphors. a) The PL spectra of ZnS:Mn^{2+} nanoparticles with different UV irradiation times. The inset shows the corresponding quantum efficiency. Reproduced with permission.[148] Copyright 2010, AIP Publishing LLC. b)The emission spectra of ruby sharp-line luminescence under pressure. A: ambient atmospheric pressure; B: 22.3 kbar; C: 40 kbar. Reproduced with permission.[149] Copyright 1972, American Association for the Advancement of Science. c) The emission intensity of ZnS:Mn/PMN-PT thin film structure as a function of frequency under an applied voltage of 10 V_{pp}. Reproduced with permission.[151] Copyright 2012, John Wiley & Sons, Inc. d) The NIR PL spectra of STO:Ni thin films with varied thicknesses and ceramic bulk under 325 nm excitation. e) The emission spectra of STO:Ni/PMN-PT under an external electric field. Reproduced with permission.[87] Copyright 2014, Nature Publishing Group. f) The emission spectra of Ni-doped silicate glass ceramic as a function of the sample temperature. Reproduced with permission.[153] Copyright 2005, AIP Publishing LLC.

presents the strain-induced emission intensity as a function of frequency under the applied voltage 10 V_{pp}. The inset shows the emission spectrum of ZnS:Mn at 10 V_{pp} and 650 kHz. The tunable luminescence intensity strongly depends on the voltage frequency, indicating that the resonance occurs at its natural frequency.

Furthermore, Ni^{2+}-doped $SrTiO_3$ (STO:Ni) thin film was grown on a piezoelectric PMN-PT substrate. Based on strain engineering, our group presented tunable luminescence of STO:Ni by two methods.[87] First, misfit strain can be modified through depositing STO:Ni films with varied thickness. Figure 10d exhibits NIR PL spectra of STO:Ni thin films and ceramic bulk excited with a 325 nm laser. Notably, the NIR emission bands from STO:Ni thin films present an obvious blueshift from 1372 to 1325 nm, and the luminescence full width at half maximum (FWHM) gradually decreases from 315 to 228 nm, when increasing film thickness. On the other hand, with decreasing the film thickness, the PL decay becomes rapid. Obviously, through controlling the thickness of the STO:Ni film, the luminescence properties of the films including emission wavelength and bandwidth as well as lifetime can be effectively tuned. The observed phenomena can be explained by the variation in the crystal field around Ni^{2+} ions, caused by misfit strain. Secondly, the modulation of strain can be provided by piezoelectric PMN-PT under an external electric field. Interestingly, with increasing applied voltage from 0 to 500 V, the emission peak position shows a blueshift from 1326 to 1313 nm, meanwhile the PL intensity gradually increases from 8.3 to 9.13 (Figure 10e).

4.2.3. Temperature-Induced Tuning

Besides pressure and stress, temperature can also modify the luminescence of transition metal ion-doped phosphors, unlike Ln ion-doped phosphors.[152] Suzuki et al.[153] fabricated transparent silicate glass ceramics with embedded Ni-doped nanocrystals for application in optical amplifiers. They found that the NIR emission intensity decreased when increasing the temperature. The PL intensity at 5 K was four times as large as that at room temperature. Meanwhile, the luminescence peak showed a slight blueshift, dependent on the temperature, namely from 1360 nm at 5 K to 1300 nm at 300 K (Figure 10f), due to temperature-induced modulation of the energy state. In addition, the effective lifetime changed from more than 900 μs at 5 K to 500 μs at 300 K. All the observed phenomena mainly result from the mechanism of temperature-dependent nonradiative relaxation.

4.3. Main Group Metal Ion-Doped Phosphors

Apart from lanthanide ions and transition metal ions, main group metal ions, including 6p (Bi, Pb) and 5p (Sb, Sn, In, Te), are promising as a new type of active ion,[154] due to the broadband NIR luminescence of main group metal ion-doped materials.[155] In particular, bismuth-doped glasses and crystals have drawn much research effort, triggered by their ultra-broadband NIR emission with a bandwidth over 300 nm, covering the whole optical fiber transmission window, with potential

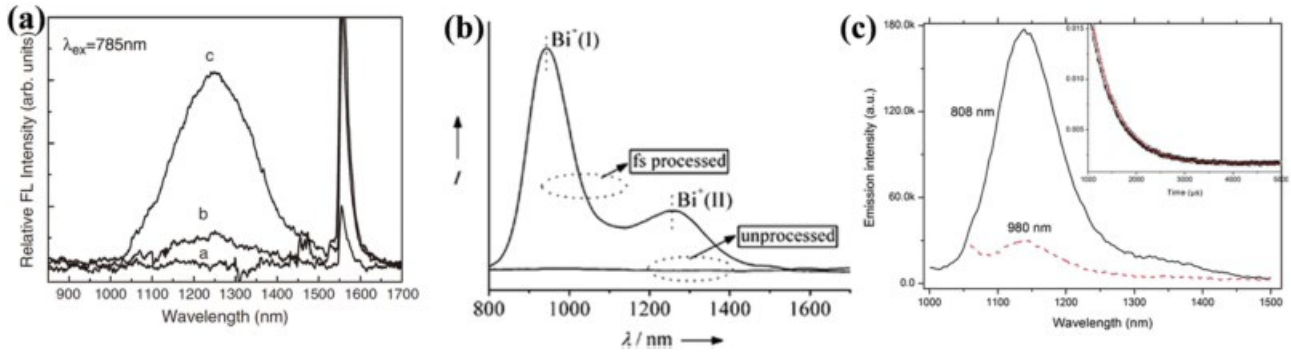

Figure 11. Tuning the luminescence of main group metal ion-doped phosphors. a) The emission spectra of Bi-doped glasses under fs laser irradiation with different energies: 'a' without irradiation; 'b' 1.0 μJ; 'c' 2.5 μJ. Reproduced with permission.[159] Copyright 2009, The American Ceramic Society. b) The emission spectra of Bi-doped glasses with and without fs laser irradiation. Reproduced with permission.[73] Copyright 2009, The Royal Society of Chemistry. c) NIR emission spectra of ©-irradiated ⟨-BBO:Bi crystal upon 808 nm and 980 nm excitation. The inset is the decay curve of the 1139 nm emission. Reproduced with permission.[160] Copyright 2009, Optical Society of America.

application in NIR-tunable light sources.[156] What is more, NIR laser outputs have been realized in single Bi-doped silica glass fibers at room temperature.[157] However, the origin of NIR emission in Bi-doped phosphors is still controversial. Several proposals have recently been made, attributing the NIR emission centers to Bi^{5+} ions, Bi^{+} ions, and Bi-ion clusters.[158] In order to carry out fundamental studies and control the valence of the Bi-ion dopant, the following physical approaches have been employed to modify Bi-doped phosphors.

4.3.1. Femtosecond Laser-Induced Tuning

Absorption and luminescence properties of Bi-doped glasses have been modulated via fs laser irradiation.[159] Through conventional melting and quenching methods, bismuthate glass with composition $52Bi_2O_3$-$23B_2O_3$-$4SiO_2$-17PbO-$4Sb_2O_3$ (wt%) was prepared. The prepared glass showed almost no absorption band in the visible or NIR ranges, and no NIR luminescence under 785 nm excitation. After fs laser irradiation, a strong absorption band appeared at around 500 nm, and peak intensity increased as the laser pulse energy was increased from 1.0 to 2.5 μJ. Accordingly, a broadband NIR emission peak arose, and the intensity was dramatically enhanced with increasing laser pulse energy (**Figure 11**a). It was deduced that the observed change results from fast, photon-induced reduction of Bi^{3+} ions to Bi^{+} ions. Under sufficiently high-intensity laser irradiation, multiple photons are simultaneously absorbed by electrons, allowing them to transfer from the valence band to the conduction band. With increasing pulse energy, the number of electrons increases and thereby the probability of permanent reduction is enhanced, leading to the increase in concentration of Bi^{+} ions, and the enhancement in NIR emission intensity.

More interestingly, a focused, ultrashort laser pulse was employed to induce multiple active centers of bismuth in the mesoporous silica glass.[73] Through porous glasses soaked in solutions of $Bi(NO_3)_3$, Bi^{3+}-doped mesoporous glasses were fabricated, as confirmed by the typical blue emission from the $^3P_1 \rightarrow {}^1S_0$ transition of Bi^{3+} ions. After fs laser irradiation, the processed area shows an intense red emission that is visible to the naked eye. The red emission can be attributed to the $^2P_{3/2} \rightarrow {}^2P_{1/2}$ transition of Bi^{2+} ions, differing from the blue emission in the unprocessed area, indicating the fast photon-induced reduction from Bi^{3+} ions to Bi^{2+} ions. With an 808 nm laser diode as a pump source, broadband NIR emission with two obvious bands at around 950 and 1235 nm is presented (Figure 11b). The NIR luminescence is associated with the $^3P_1 \rightarrow {}^3P_0$ transition of Bi^{+} emission centers. In contrast, there is no NIR emission in the unprocessed area. Based on the observed PL spectra, some of the Bi^{3+} ions should be photoreduced to lower valence states, i.e., Bi^{2+} and Bi^{+} ions, under fs laser irradiation. It is suggested that the multiphoton absorption process and photoreduction of Bi^{3+} ions are involved in the experimental phenomenon. Through Joule heating, multiphoton ionization, and collisional ionization, free electrons are created in the fs laser-focused area. After that, Bi^{3+} ions capture the free electrons and hence transform into Bi^{2+}, and even Bi^{+} ions. The holes would be trapped at nonbridging oxygens in the SiO_4 polyhedrons. Note that $Bi^{3+} + e \rightarrow Bi^{2+}$ and $Bi^{2+} + e \rightarrow Bi^{+}$ are very similar to the conventional chemical processes. It is suggested that control of the laser parameters can tune the active centers for the luminescence tuning of main group metal ion-doped phosphors.

4.3.2. ©-Ray Irradiation-Induced Tuning

Besides tuning by fs laser irradiation, luminescence of main group metal ion-doped phosphors can be modulated by ©-ray irradiation. Bi-doped ⟨-BaB_2O_4 (⟨-BBO) single crystals were prepared through the Czochralski method in an N_2 atmosphere.[160] The absorption and PL spectra of as-grown crystals indicate that Bi^{2+} and Bi^{3+} centers occur in the hosts. There was no NIR luminescence in the as-grown Bi-doped crystals under 808 nm or 980 nm laser diode excitation. In contrast, intense NIR emission was observed in the ©-ray-irradiated Bi-doped ⟨-BBO (Figure 11c). Bi^{+} ions were considered NIR luminescent centres. Under ©-ray irradiation, the electrons can be easily released from the Ba vacancies (V_{Ba}3), and would freely displace in the lattice. Then, the Bi^{2+} and Bi^{3+} ions would capture the free electrons and transform to Bi^{+} centres. Interestingly, the ©-ray-irradiated Bi-doped ⟨-BBO can be bleached by heat

annealing, due to the processes of $Bi^{+} \square 2e \square \square Bi^{3+}$ and $V_{Ba} + 2e \square \square V_{Ba}3$. Similarly, NIR luminescence from ©-ray-irradiated Bi-doped Y_4GeO_8 crystals was investigated.[161]

5. Nanostructured Semiconductors

Differing from metal ion-doped phosphors, the luminescence of semiconductors is strongly dependent on the band-edge and bound excitons. Decreasing the dimensionality of semiconductors to the nanoscale in one, two, or three directions leads to thin-film structures (2D), wires (1D), or dots (0D), respectively. Striking electronic properties of nanostructured semiconductors depend qualitatively on details of the geometry of the structure (shape and size) and of the distribution of atoms inside. The electronic properties, in turn, control the luminescence properties. Thus, control over the geometrical architecture opens enormous opportunities for designing novel semiconductor phosphors. These opportunities extend far beyond a conventional chemical approach, where properties are mainly modulated by varying the chemical composition. Once synthesized, the optical properties of nanostructured semiconductors are normally fixed and cannot be easily tuned further. Hence, it would be attractive to control the luminescence of nanostructured semiconductors by physical methods. In fact, tuning the luminescence of nanostructured semiconductors has been reported, with the aid of an external electric field,[162] a magnetic field,[163] plasmons,[164] and mechanical stress.[165] Through varying the band-edge and bound excitons by these physical methods, the luminescence properties of nanostructured semiconductors can be tuned without any need to change the samples.

5.1. Quantum Dots

Semiconductor QDs have generated considerable interest in optoelectronics and biotechnology because of their small sizes, narrow band emission, high quantum efficiency, and spectral tunability.[166] With the unusual behavior of quantum confinement, the luminescence properties of QDs have routinely been modulated by changing their morphology and size during preparation.[167] After synthesis, the luminescence properties of QDs may possibly be controlled using some physical methods, such as electric and magnetic fields.[168]

5.1.1. Electric-Field-Induced Tuning

Based on the quantum-confined Stark effect, tunable luminescence of single nanocrystallite QDs was observed under an external electric field. Empedocles and Bawendi[47] applied electric fields to interdigitated Ti–Au electrodes on a quartz substrate. Then, a dilute solution of CdSe QDs was placed over the electrodes. Spectra were taken from QDs located midway between neighboring electrodes to ensure a uniform electric field. With the external electric field either on or off, the single emission peak is presented from the same single dot corresponding to the zero phonon line, which can shift between two distinct energies in response to the electric field at 10 K (**Figure 12**a). This shift is real-time and highly reproducible in nature, and is much greater than the linewidth. As shown in Figure 12b, the relationship between the Stark shift and the electric field can be well fitted with Equation (2) presented in Section 3. With changes in the applied electric field, the emission peak shifts as much as 75 meV for a single QD

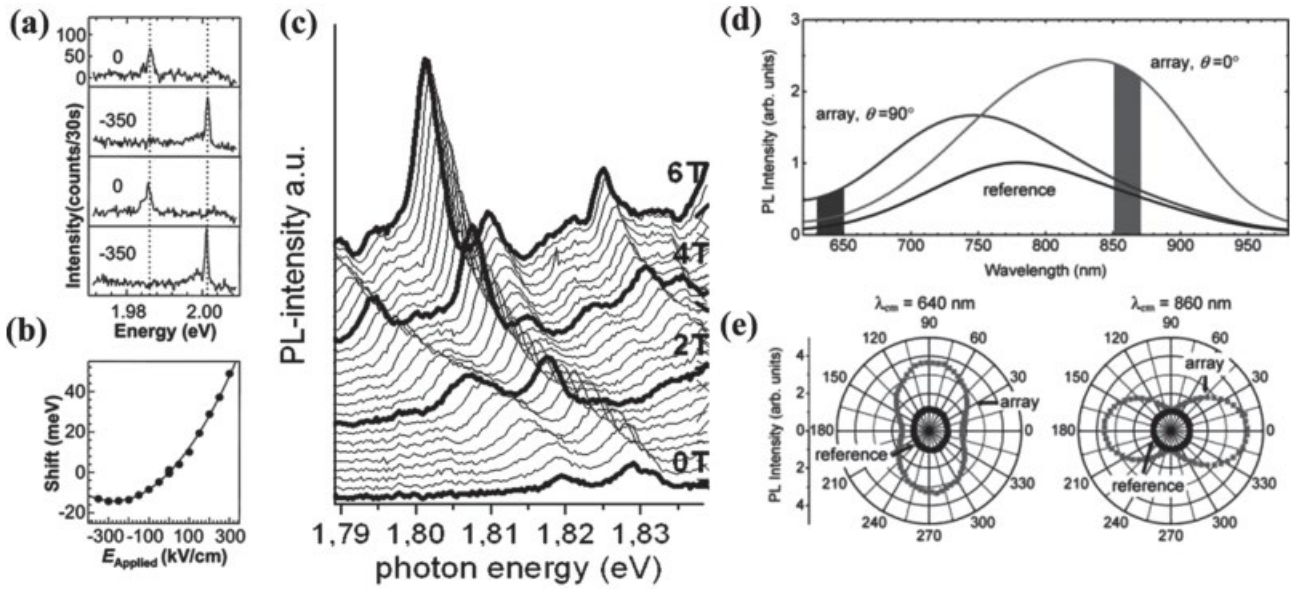

Figure 12. Tuning the luminescence of QDs. a) The emission spectra of QDs under an alternating electric field. b) The emission shift as a function of the applied electric field. Reproduced with permission.[47] Copyright 1997, American Association for the Advancement of Science. c) The PL spectra from a single CdTe:Mn QD under an external magnetic field from 0 to 6 T. Reproduced with permission.[169] Copyright 2007, The American Physical Society. d) Si quantum-dot PL spectra measured on the reference area and on the array, the latter for two emission polarization angles \. e) The polar plots of the Si QD PL intensity as a function of \ of the emission measured both on the array and the unpatterned reference area for λ_{em} = 640 nm and λ_{em} = 860 nm. Reproduced with permission.[171] Copyright 2006, American Chemical Society.

of ZnS-over-coated sample (CdSe radii: 37.5 Å; ZnS shell thickness: 6 Å). These applied local fields result in spontaneous spectral diffusion and contribute to ensemble inhomogeneous broadening. The observation indicates the potential application of these kinds of dots in electro-optic modulation devices. In contrast to electric field-induced tuning in Ln ion-doped phosphors at room temperature,[51] this measurement was carried out at low temperature for stabilizing QDs.

5.1.2. Magnetic-Field-Induced Tuning

Through introducing magnetic metal ions into QDs, QDs could exhibit magnetic properties. The possibility of magnetic QDs with giant Zeeman splitting allows one to tune their emission using an external magnetic field.[169] An interesting example is the luminescence of diluted magnetic QDs, which can be modulated by an external magnetic field. Magnetic QDs were fabricated by Wojnar and co-workers,[170] through introducing Mn ions into CdTe QDs. By increasing the magnetic field, the PL line from a single CdTe QD doped with 3.5% Mn shows a clear redshift and spectral narrowing (Figure 12c). The energy shift of the magnetic QD at 6 T reaches up to 28 meV. This measurement implies giant Zeeman splitting of the excitonic levels inside the dots, associated with the sp–d exchange interaction between carriers confined inside the dot and transition metal Mn ions. In contrast to the above Ln ion-doped phosphors, magnetic-field-induced tuning of QDs can result in a shift of the emission wavelength.

5.1.3. Plasmon-Induced Tuning

Through coupling the Si QDs to elongated silver nanoparticles, the PL intensity of the Si QDs is plasmon-enhanced in a polarization-selective way. Mertens and co-workers[171] fabricated elongated Ag nanoparticles utilizing electron-beam lithography on top of prepared Si-QD-doped silica substrates. The typical diameter of the formed Si QDs is 2–5 nm, while the fabricated Ag nanoparticles have the dimensions 240 · 140 · 20 nm3. They found that the fabricated Ag nanoparticle array presented polarization-dependent extinction spectra, stemming from the anisotropic particle dimensions. The extinction spectrum parallel to the sample ($\theta = 0°$) presents a peak at 860 nm, whereas the extinction spectrum perpendicular to the sample ($\theta = 90°$) reaches its maximum around 640 nm. The nanoparticle surface charge distributions produced by plane-wave illumination are dissimilar for the two polarizations. As a result, different restoring forces are created, which induces blueshifting and redshifting of the resonance frequencies for the transverse and longitudinal polarizations, respectively. The dipolar plasmon modes of the Ag nanoparticles are speculated to dominate the extinction. More importantly, the PL spectra measured of the nanoparticle array show exceptional changes compared with unpatterned reference areas (Figure 12d). The luminescence of Si QDs is improved in a strongly wavelength- and polarization-dependent way. The maximum enhancement at the emission wavelengths of $\lambda_{em} = 640$ nm for $\theta = 90°$ and $\lambda_{em} = 860$ nm for $\theta = 0°$ exceeds a factor of three (Figure 12e). The polarization-selective PL enhancement was confirmed from polar plots of the Si-QD PL intensity-dependent θ of the emission, which is measured both on the array and the unpatterned reference area for $\lambda_{em} = 640$ nm and $\lambda_{em} = 860$ nm. Such emission enhancement can be interpreted by the electromagnetic coupling of the Si-QD emission dipoles with dipolar plasmon modes of the Ag nanoparticles. This approach implies that engineered plasmonic nanostructures can be used to optimize and modulate the performance of phosphors, not only by enhancing adsorption and emission rates, but also by affecting the polarization of the emission.

Wu's group[172] reported the tuning of colour patterns of QDs based on LSP resonance and photoactivation effects. They fabricated PMMA-CdSe QDs in toluene solution and a Si wafer with half the area coated in a 60-nm Ag film. Then, PMMA-QD films and Ag-QD coupling systems were prepared by spin-coating the solutions onto the wafer. After annealing, a large enhancement of the PMMA-QD/Ag area was found compared with the reference area. The colour change and the quantum yield (QY) of the samples increases from 0.73% to 14.9% (**Figure 13**a). Accordingly, the inset of the figure indicates vivid colour and brightness contrast between the two areas. This result was explained by the coupling effect of the radiative surface state emissions (SSEs) from the QD/Ag area and LSPs on the Ag nanostructures. Under UV irradiation (Figure 13b), the band-edge emission intensities of the two areas are obviously enhanced compared with Figure 13a. The QYs for the QD/Ag and reference areas are 21.0% and 5.8%, respectively. Hence, the colour was dependent on the band-edge emission in the area without Ag, whereas the colour of the QD/Ag area was dominated by the enhanced SSE. Therefore, LSP resonance and photoactivation effects can be utilized to tune the colour and QY of QDs.

5.1.4. Mechanical Stress-Induced Tuning

Through applying strain to QDs during fabrication, the emission energy of the QDs can be shifted significantly. Recently, using the piezoelectric effect of certain substrates (lead zirconium titanate (PZT), PMN-PT), Schmidt and co-workers utilized an external perturbation in situ to apply controllable stress to QDs.[173] The emission energy of QDs can be reversibly tuned to lower and higher values. The stress from a piezoelectric material can result in band-structure tuning, fine-structure splitting and, as a consequence, the emission energy modulation of QDs. For instance, a thin *n-i-p* nanomembrane containing InGaAs QDs was integrated onto PMN-PT piezoelectric actuators by Au thermocompression bonding.[86] A voltage applied to PMN-PT allows the in-situ application of anisotropic biaxial strains in the *p-i-n* nanomembrane by controlling the electric field (F_p). Independently, a bias voltage (V_d) applied to the nanomembrane allows a high electric field (F_d) across the diode. The two tuning knobs were used for detecting the emission data presented in the inset of Figure 13c. This figure presents a μ-EL map of a single QD as a function of the setting V_d. When V_d goes above the turn-on voltage of the *p-i-n* diode, charge carriers are injected into the QDs, and photons with different wavelengths are released in the recombination processes. Figure 13d presents several μ-EL spectra of a single QD with

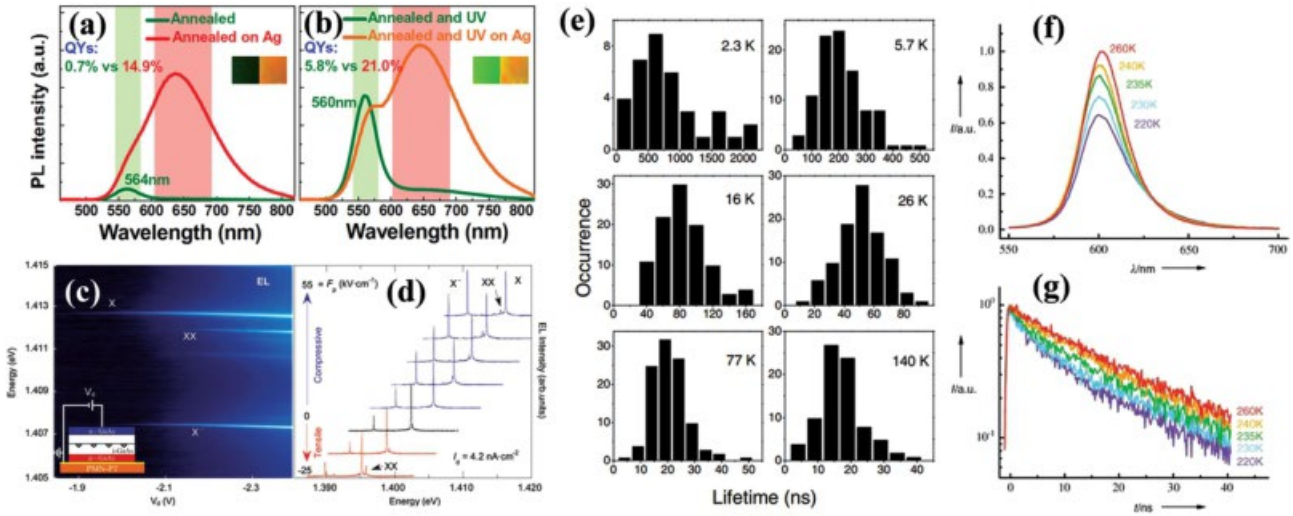

Figure 13. Tuning the luminescence of QDs. a) The PL spectra of the PMMA-QD/Ag area and the reference area. b) The PL spectra of the PMMA-QD/Ag area and the reference, after UV irradiation. Reproduced with permission.[172] Copyright 2012, IOP Publishing. c) μ-EL map of a single QD as a function of setting V_d. d) Several μ-EL spectra of a single QD with a fixed current flow as a function of setting F_p. Reproduced with permission.[86] Copyright 2012, John Wiley & Sons, Inc. e) The luminescence lifetime of single CdSe/ZnS QDs at different temperatures. f) The PL spectra of hexylamine-capped CdSe QDs with increasing temperature. Reproduced with permission.[174] Copyright 2003, The American Physical Society. g) The PL decay curves of hexylamine-capped CdSe QDs with an increase in temperature. Reproduced with permission.[175] Copyright 2004, John Wiley & Sons, Inc.

a fixed current flowing as a function of the setting F_p. Under tensile stress, the emission peaks show redshifts, whereas compressive stress induces blueshifts. The large emission tuning in the same sample results from the structural change of the individual QDs induced by the stress from piezoelectric crystal, PMN-PT. More interestingly, due to the combination of the external electric and strain fields, the QD luminescence properties can be engineered through controlling the fine-structure splitting.

5.1.5. Temperature-Induced Tuning

Temperature is another possible approach to modulate the luminescence of QDs. Labeau et al. have investigated the effect of temperature on the luminescence lifetime of single CdSe/ZnS QDs.[174] Measurements of lifetimes were carried out at various temperatures (between 2.3 and 140 K) on about 100 single QDs with a time-correlated single-photon counting technique. The mean decay rate increases with temperature and saturates at temperatures of above 70 K. The mean count rate detected from single QDs decreases remarkably below this temperature (Figure 13e). These results indicate that the photon emission originates from two thermally populated states, including a weakly emissive long-lived ground state and a strongly emissive upper one. Normally, the measurement of QDs is performed at low temperatures compared to those used to characterise the above-introduced bulks of metal ion-doped phosphors.

In general, the QY of QDs gradually decreases as the temperature increases, an effect known as temperature quenching. However, Wuister and co-workers[175] found that the QY of capped CdSe QDs increases greatly when the capped QDs are heated above a definite temperature, named the antiquenching temperature. Taking hexylamine-capped CdSe QDs as an example, when increasing the temperature from 220 to 260 K, the PL intensity gradually increases and the PL decay becomes continuously slower (Figure 13f,g). The observed temperature antiquenching was deduced to be due to the organic layer-induced passivating dangling lone pairs, as well surface reconstruction.

5.2. Quantum Wells

Qunatum wells (QWs) are formed in semiconductors with thin film heterostructures. As a quasi-2D system, the optical properties of QWs are quite different from those of bulk semiconductors. Due to the unique optical properties, QWs play an important role in optoelectronic devices, such as semiconductor laser, LEDs, photodetector, and so on.[68,176] So far, some groups have reported luminescence tuning of QWs through external fields.

5.2.1. Electric Field-Induced Tuning

One of the typical luminescence modulations by an external electric field was shown by Mendez and co-workers. They measured PL spectra of GaAs QWs of $L_z = 30$ Å with a He–Ne laser (632 nm), under an applied electric field perpendicular to the wells. For an external voltage of +0.73 V, two well-defined emission bands were found at 737.6 and 746 nm (**Figure 14**a).[176] The former band is attributed to a free exciton recombination process between the electrons and the heavy hole ground states of the QWs. The latter one is most probably due to the recombination of the $n = 1$ free electrons with the acceptor carbon in the MBE grown samples. Decreasing the external voltage, the intensity of both bands decreases, with the one at higher

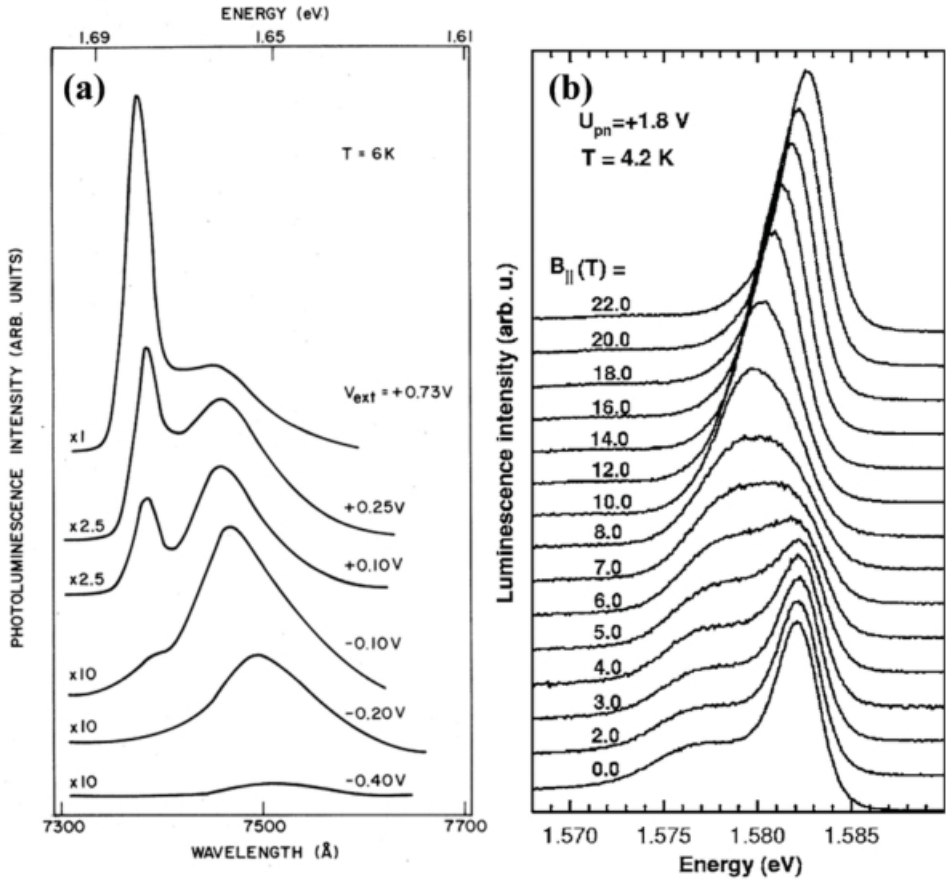

Figure 14. Tuning the luminescence of QWs. a) The PL spectra of GaAs QWs pumped at 632 nm under an external electric field perpendicular to them. Reproduced with permission.[176] Copyright 1983, Elsevier B.V. b) Normalized PL spectra of DQW at a constant bias of U_{pn} = +1.8 V, in the in-plane magnetic field (B_t). Reproduced with permission.[178] Copyright 2005, The American Physical Society.

energy decreasing more quickly. The exciton peak is almost completely quenched when the voltage reaches □0.2 V, and the impurity band almost disappears when the applied voltage is below □0.4 V. Meanwhile, both peaks exhibit a redshift as the external voltage decreases. The quenching of the luminescence is related to the spatial separation of charge carriers induced by the applied electric field. The recombination probability is therefore effectively tuned. The shift of the emission peaks results from the effect of the field on the energy position of the quantum states.

5.2.2. Magnetic Field-Induced Tuning

Huang and Lyo predicted that PL line shapes of *n*-doped double quantum wells (DQWs) could be sensitively modulated by an applied parallel magnetic field at low temperature.[177] Under the in-plane magnetic field, Orlita and co-workers[178] indeed observed the modulated luminescence of DQWs at low temperature. Figure 14b shows the parallel magnetic field (B_t) dependence of PL spectra at a constant bias U_{pn} = +1.8 V. The shape of the two PL peaks at B_t = 0 is due to the recombination energies for electrons in the bottom of the bonding (B) and antibonding (A) sub-bands, with heavy holes localized in the potential fluctuations. The spectra under increasing B_t reveal a gradual damping of the emission line arising in sub-band A. Around B_t = 7.0 T, the emission from the sub-bands is quenched completely, because of the totally diminished recombination. Further increasing B_t causes a further narrowing of the PL band as well as a peak blueshift. Consequently, it can be seen that the luminescence of DQWs, in terms of the emission energy and PL profile, can be altered by an in-plane magnetic field.

5.2.3. Plasmon-Induced Tuning

Scherer's group reported an interesting result of SP-enhanced light emission from InGaN QWs.[69] They coated several different types of metal layers onto InGaN/GaN QWs, as shown in Figure 5b. Ag, Al, and Au layers were utilized, and the distance between the metal layer and the QW was 10 nm in each case. **Figure 15**a presents typical PL spectra of the metal layer-coated QWs. Note that the PL peak intensity of the uncoated reference QW at 470 nm is normalized to 1. Compared with the reference emission, the Ag-coated emitter is enhanced the most: a 14-fold enhancement in the PL peak intensity is seen, whereas only an 8-fold peak intensity is achieved for the Al-coated QW. Almost no peak intensity

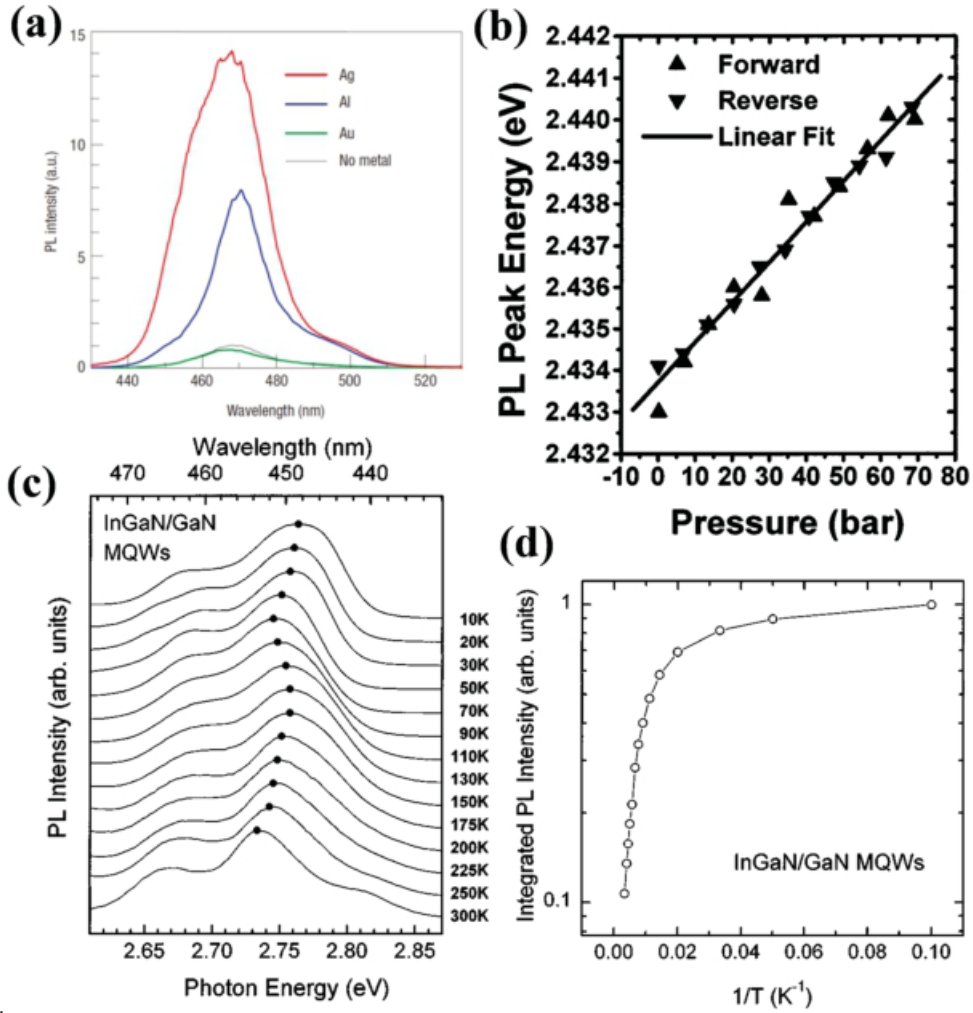

Figure 15. Tuning the luminescence of QWs. a) The PL spectra of InGaN/GaN QWs coated with Ag (red curve), Al (blue curve), and Au (green curve). The PL peak intensity of uncoated QWs at 470 nm was normalized to 1. Reproduced with permission.[69] Copyright 2004, Nature Publishing Group. b) PL peak energy of InGaN QW as a function of the applied pressure. Reproduced with permission.[180] Copyright 2000, AIP Publishing LLC. c) The PL spectra of InGaN/GaN multiple quantum wells (MQWs) under different temperature. d) Integrated PL intensity as a function of 1/T in InGaN/GaN MQWs. Reproduced with permission.[183] Copyright 1998, AIP Publishing LLC.

enhancement is observed for the Au-coated one. The results suggest that Ag is suitable for SP coupling to blue emission. The estimated plasmon energy of the coated Ag layer is about 3 eV (410 nm), which is close to its emission. Thus, luminescence from Ag-coated samples is enhanced due to resonant SP excitation. The estimated plasmon energy of Au on GaN is below 2.2 eV (560 nm), so no measurable enhancement is detected in the Au-coated sample owing to the mismatch between the SP and QW energies. In addition, they found that the PL enhancement ratio is strongly dependent on the distance between the QW and the metal layer coating. Ag and Al samples present exponential increases in the PL intensity as the distance decreases. The SP enhancement of QW emission provides an effective way to develop highly efficient light sources. Very recently, through coupling the hot excitons in AlGaN-based QWs with the plasmon energy-matched Al nanoparticles, the deep UV emission showed a 3.2-fold enhancement.[179]

5.2.4. Mechanical Stress-Induced Tuning

Through applying strain on QWs, their luminescence can be tuned due to the energy gap change or the built-in electric field modulation. Aumer and co-workers[180] modulated the luminescence properties of AlInGaN/InGaN QW using misfit strain, including both tensile and compressive strain. Shapira et al. applied biaxial strain to a typical InGaN QW and the luminescence peak energy was controlled.[181] The PL peak position blueshifted linearly as the pressure increased, and redshifted with no hysteresis as the pressure decreased (Figure 15b). A strain-induced reduction was proposed to lead the blueshift of the emission peak.

5.2.5. Temperature-Induced Tuning

QW-based semiconductors are usually used for LED applications, and it is therefore of vital importance to investigate the

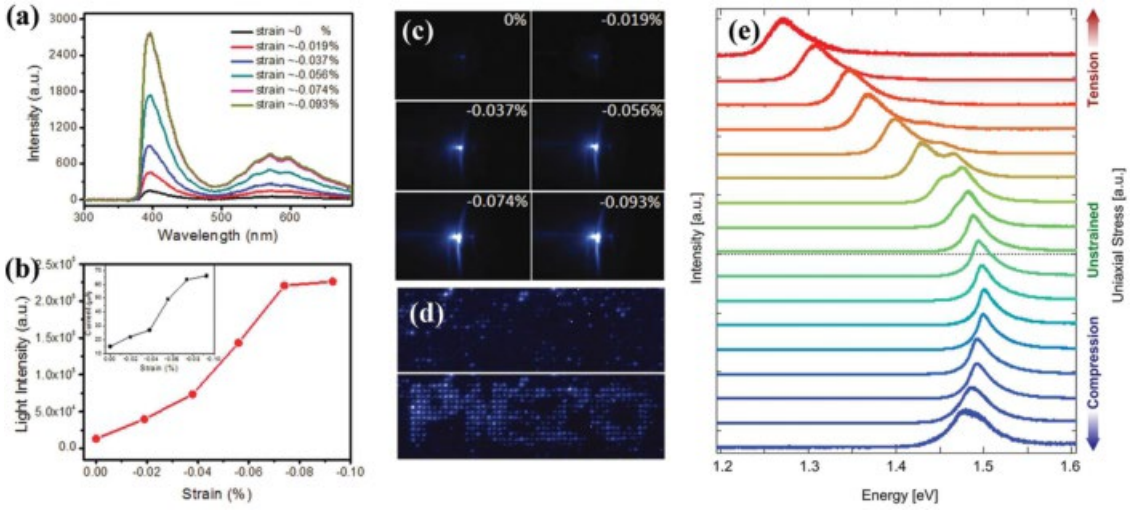

Figure 16. Tuning the luminescence of nanowires. a) The EL spectra of a ZnO wire LED under strain at a bias of 9 V. b) The strain-dependent light emission intensity. c) Photographs of the nanowire LED under different applied strains. Reproduced with permission.[186] Copyright 2011, American Chemical Society. d) Photographs of the prepared nanowire LED array with (down) and without (top) a convex character pattern of 'PIEZO' mould applied. Reproduced with permission.[187] Copyright 2013, Nature Publishing Group. e) The normalized PL spectra of an individual nanowire are plotted as a function of energy for different values of applied uniaxial stress. Reproduced with permission.[88] Copyright 2013, American Chemical Society.

impact of temperature on the QW structures. Eliseev et al. studied the temperature dependence of single-QW-structured EL and PL spectra of light-emitting AlGaN/InGaN/GaN in the temperature range 40–270 K.[182] Blueshifting of the emission peaks was measured in both types of emission spectra. Such a phenomenon is considered due to the distribution of the density of states with a Gaussian band tail. In a later work, Cho et al. reported an 'S-shaped' temperature-dependent emission shift and carrier dynamics in InGaN/GaN multiple QWs.[183] The PL spectra showed different red/blueshifts of the peak wavelengths (λ_p) and bandwidths at different temperature ranges. For example, the λ_p redshifts for 10–70 K, blueshifts for 70–150 K, and redshifts again for 150–300 K (Figure 15c). In addition, the bandwidth narrows when λ_p redshifts and vice versa. The shifts were caused by a change in the carrier dynamics with increasing temperature, due to inhomogeneity and carrier localization in the InGaN/GaN multiple QWs. In Figure 15d, the emission intensities were also quenched upon increasing temperature because of thermionic emission from photocarriers out of the potential minima.

5.3. Nanowires

Semiconductor nanowires are of great interest due to their promising application in laser diodes, LEDs, waveguides, and other photonic devices.[184] Compared to bulk semiconductors, the high-yield strength and exotic mechanical properties of nanowires make them a very attractive system for tuning emission with external stimuli, including mechanical stress and temperature.

5.3.1. Mechanical Stress-Induced Tuning

Benefiting from the piezo-phototronic effect of ZnO nanowires or microwires, enhanced light emission from strained LEDs has been presented by Wang's group.[185] The effect of strain on the light emission of an LED was evaluated in a (*n*-ZnO wire)–(*p*-GaN film) device.[186] At a fixed bias above 3 V of turn-on voltage, both current and EL intensity (**Figure 16**a,b,c) are obviously improved with increasing compressive strain. When applying a 0.093% *a*-axis compressive strain, the enhancement factors of light emission intensity and injection current can reach up to 17 and 4, respectively. According to the piezo-phototronic effect, the key operation principle is that the strain can create a piezopotential in ZnO with a non-centrosymmetric structure, resulting in the charge carrier separation, transport, and recombination processes. Then, the light emission and injection current are enhanced upon increasing the applied strain. A nanowire LED array with the ability to map the pressure distribution was fabricated and demonstrated by Pan et al.[187] A convex character pattern of 'PIEZO' mould was directly applied onto the LED arrays, in order to present 2D mapping of the strain. Images of light emission of the nanowire device under the applied strains from 0% to □0.15% were collected by a charge-coupled device (CCD). With increasing compressive strain, the device directly exhibits the word "PIEZO", while those not affected by the character pattern presented almost no change in light emission (Figure 16d). As each nanowire LED is a pixel, the spatial resolution is 2.7 μm, indicating that this piezoelectric nanowire LED array can map 2D pressure distributions in high resolution. Consequently, the piezo-phototronic effect used by Wang provides an opportunity to improve the performances of various optoelectronic devices.[81]

Signorello and co-workers have investigated the effect of uniaxial stress on the luminescence of GaAs/$Al_{0.3}Ga_{0.7}As$/GaAs core/shell/shell nanowires.[88] According to a three-point bending mechanism (Figure 7d), uniaxial compressive and tensile stresses could be applied to the nanowire in a continuous, real-time, and reversible way. Meanwhile, PL spectra were measured with a He–Ne laser as a function of

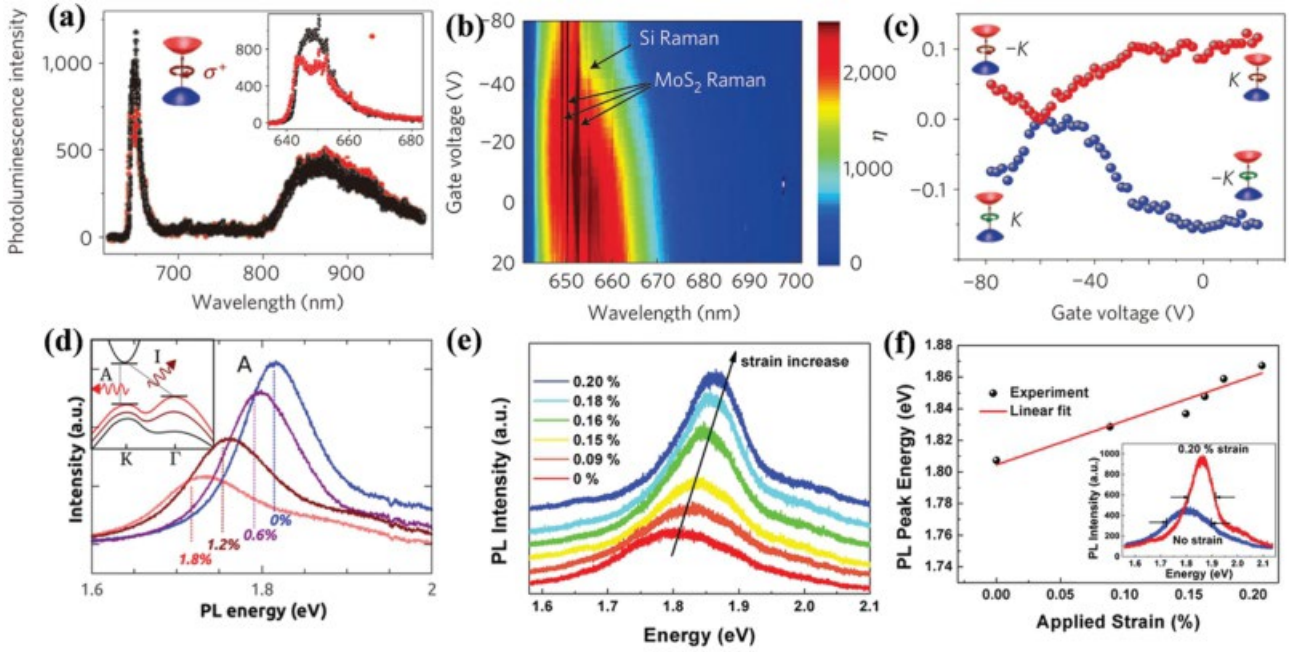

Figure 17. Tuning the luminescence of atomic-layered 2D nanomaterials. a) The polarization-resolved μ-PL spectra of bilayer MoS_2 FETs under $\int_+$ polarized light excitation, $V_g = 0$. b) The $\int_+$ light emission map under $\int_+$ excitation when decreasing V_g from positive to negative. c) The polarization | at 648 nm as a function of V_g. Reproduced with permission.[193] Copyright 2013, Nature Publishing Group. d) The emission spectra of monolayer MoS_2 under various strains. Reproduced with permission.[194] Copyright 2013, American Chemical Society. e) The emission spectra of trilayer MoS_2 sheets under various strains. f) The PL peak energy of trilayer MoS_2 sheets as a function of applied strain. Reproduced with permission.[195] Copyright 2013, American Chemical Society.

the stress applied to the nanowires. As shown in Figure 16e, the normalized PL spectra of an individual nanowire are plotted as a function of energy for different values of applied uniaxial stress. Under compression, the unstrained peak around 1.48 eV shows a slight and nonlinear shift with an increase in stress, and the peak width broadens as well. A much stronger redshift toward lower energies and peak splitting are observed when tensile stress is applied. The tuning range up to 296 meV with increasing stress is measured in the strained nanowires. Compared with the above-introduced bulk metal ion-doped phosphors, tuning the luminescence by mechanical stress is more effective in semiconductor nanowires.

5.3.2. Temperature-Induced Tuning

The temperature-dependent PL of single GaAs/AlGaAs core/shell nanowires was investigated by Titova et al.[188] When increasing the temperature from 10 to 120 K, the emission of a nanowire redshifts and broadens and is strongly quenched as the temperature approaches 120 K. The temperature dependence of the peak energy of nanowires and of bulk GaAs are reported. The data can be well fitted with the modified Varchni equation. The fit for the nanowires is significantly different to that of the bulk. In particular, the linear slopes of the curves for nanowires are obviously shallower than those of the bulk. It is suggested that increasing the temperature induces strain or different phonon responses for nanowires.

5.4. Atomic-Layered 2D Nanomaterials

Nowadays, graphene and graphene-like 2D atomic crystals have been considered potential candidates for next-generation electronics and optoelectronics, because of their amazing structural, electrical, and optical properties.[189] Differing from gapless graphene, a variety of 2D-layered semiconductors have bandgaps. In particular, 2D-layered MoS_2 (as one of the transition metal dichalcogenides) presents a strong PL, a high current on/off ratio in field-effect transistors (FETs), and LEDs.[190] Moreover, tuning the luminescence of 2D-layered MoS_2 via electrical tuning of valley magnetics[191] and strain-induced bandgap changes[192] has been observed.

5.4.1. Electric Field-Induced Tuning

With mechanically exfoliated 2D-layered MoS_2, FETs in which the back-gate voltage V_g controls the vertical electric field are fabricated. Polarization-resolved μ-PL spectra are taken from 2D-layered MoS_2 FETs using different V_g values and an excitation laser (632 nm), at a temperature of 30 K.[193] **Figure 17**a presents the polarization-resolved μ-PL spectra of bilayer MoS_2 FETs under $\int_+$ polarized light excitation, with $V_g = 0$. Here, $\int_+$ and $\int_\square$ represent the right- and left-hand-polarized signals, respectively. Note that the broad band around 860 nm originating from phonon-assisted, indirect interband transitions shows no circular polarization. Compared to the emission peak at 650 nm from direct transitions in $\pm K$ valleys with circular polarization, the band at 860 nm provides a nonpolarized reference signal.

For σ+ light excitation, the PL intensity of σ+ at 648 nm ($P(\sigma+)$) is larger than that of σ− ($P(\sigma-)$), and vice versa. The degree of circular polarization is expressed by ρ = ($P(\sigma+) - P(\sigma-)$)/($P(\sigma+) + P(\sigma-)$). The nonzero PL polarization at $V_g = 0$ indicates the existence of a broken inversion symmetry in the fabricated bilayer MoS_2. When decreasing V_g from positive to negative, the σ+ light emission under σ+ excitation shows a slight blueshift and its intensity decreases (Figure 17b). Interestingly, the polarization ρ at 648 nm exhibits a remarkable change as a function of V_g (Figure 17c). The values of ρ against V_g for σ+ and σ− excitation form a striking X-shaped pattern. The PL polarization completely disappears at the point of intersection when $V_c = -30$ V, and linearly increases with increasing or decreasing V_g from this point. Furthermore, ρ seems to approach saturation (±15%) when $|V_g - V_c| \varepsilon 30$ V. The results can be understood as electrical tuning of orbital magnetic moments through symmetry control. In sharp contrast, polarization-resolved μ-PL spectra of monolayer MoS_2 FETs show no gate dependence, due to the non-centrosymmetric structure. Hence polarization-resolved luminescence of bilayer MoS_2 can be effectively tuned by an electric field.

5.4.2. Mechanical Stress-Induced Tuning

Through strain-induced bandgap engineering, tuning the luminescence of 2D-layered MoS_2, including the emission energy and intensity, has been reported by some groups. For example, Conley et al. show that uniaxial tensile stress can greatly modulate the emission of monolayer and bilayer MoS_2.[194] They fabricated monolayer and bilayer MoS_2 flakes with Ti clamps attaching them to flexible substrates. Then PL spectra of 2D-layered MoS_2 under tensile stress were measured by employing a bending stage. The spectra of strained monolayer MoS_2 indicate a redshift of the emission peak which is approximately linearly with increasing strain, at a rate of H45 meV/% strain. Meanwhile, the peak intensity decreases to a third of the unstrained sample with an applied strain of 2% (Figure 17d). In the bilayer MoS_2, the emission peak from the direct transition is redshifted by H120 meV/% strain. The emission band originating from the transition across the indirect bandgap of bilayer MoS_2 also shows a redshift, at a rate of H50 meV/% strain. The tuning of luminescence properties can be explained by strain-induced bandgap modulation, phonon softening, and a transition from a direct band to an indirect band in strained 2D-layered MoS_2. Through employing piezoelectric PMN-PT, Lau's group observed exceptional tuning of the luminescence in a compressively strained trilayer MoS_2 sheet.[195] The trilayer MoS_2, prepared by chemical vapor deposition, was transferred onto PMN-PT (001) and covered by monolayer graphene as the top transparent electrode. In the unstrained state, a PL band around 1.8 eV was observed, which can be ascribed to the direct band transition of the trilayer MoS_2 sheet. With increasing strain, the emission peak redshifts approximately linearly, at a very large rate of H300 meV/% strain (Figure 17e,f). This tunability is the highest value ever reported for strained semiconductors. Apart from the shift in emission band, the PL emission intensity is enhanced by up to H200% and the FWHM is reduced by about 40% when increasing the strain up to 0.2%. Thus, taking advantage of controllable biaxial strain from the PMN-PT substrate, the luminescence of 2D-layered semiconductors can be effectively tuned.

6. Stimuli-Responsive Organic Phosphors

Although the industrial production quantities of inorganic phosphors have been far higher than those of organic phosphors so far, some types of organic phosphors are becoming more and more important in practical applications. In particular, dramatic developments in polymer science are enabling the design, fabrication, functional architecture, and application of novel organic phosphors. Nowadays, there are many kinds of organic and organic–inorganic hybrid phosphors, such as organic crystals and metal–organic frameworks. Some reviews related to this area have already been published, and interested readers can refer to these references.[196] Here, we will mainly focus one an emerging area, namely, stimuli-responsive polymers.

Stimuli-responsive luminescent polymers are of great interest in terms of scientific research and their promising application in photodetection, memory, sensing, and display devices. In general, stimuli-responsive luminescent polymers with dynamic molecular architectures are capable of responding to external stimuli[197] (e.g., pH changes, electric or magnetic fields, mechanical stress, and temperature), and this molecular level response is directly linked to the optical properties.[198] This inspires one to investigate whether the luminescence of this kind of polymer is capable of responding external stimuli.

The aggregation of luminophores often leads to partial or even complete quenching of their light emission. This aggregation-caused quenching (ACQ) effect has ever been a barrier to the development of organic phosphors, limiting their application scope.[199] Fortunately, Tang et al. reported a novel aggregation-induced emission (AIE) phenomenon in some organic compounds containing propeller-like molecules, such as silole and tetraphenylethene (TPE).[200] In contrast to the conventional ACQ phosphors, AIE phosphors can emit more intensely after aggregation. Recent theoretical and experimental studies indicate that the AIE phenomenon mainly originates from the restriction of intermolecular rotation. Based on this AIE effect, the luminescence of AIE phosphors can be tuned by mechanical grinding, temperature, and so on.[201]

6.1. Mechanical Stress-Induced Tuning

The modulation of luminescence of organic phosphors via a physical approach has been an attractive target for both fundamental research and applications.[202] However, the published reports are still limited compared to those using chemical routes.[203] Among the reported results, one noteworthy type of organic phosphor with piezochromic luminescence shows fantastic features among stimuli-responsive luminescent polymers.[204] Piezochromic luminescence means that PL molecular assemblies change their colour under a mechanical stimulus, including grinding, shearing, and pressing, and reverse to the original colour by recrystallization or heating.[205] For instance,

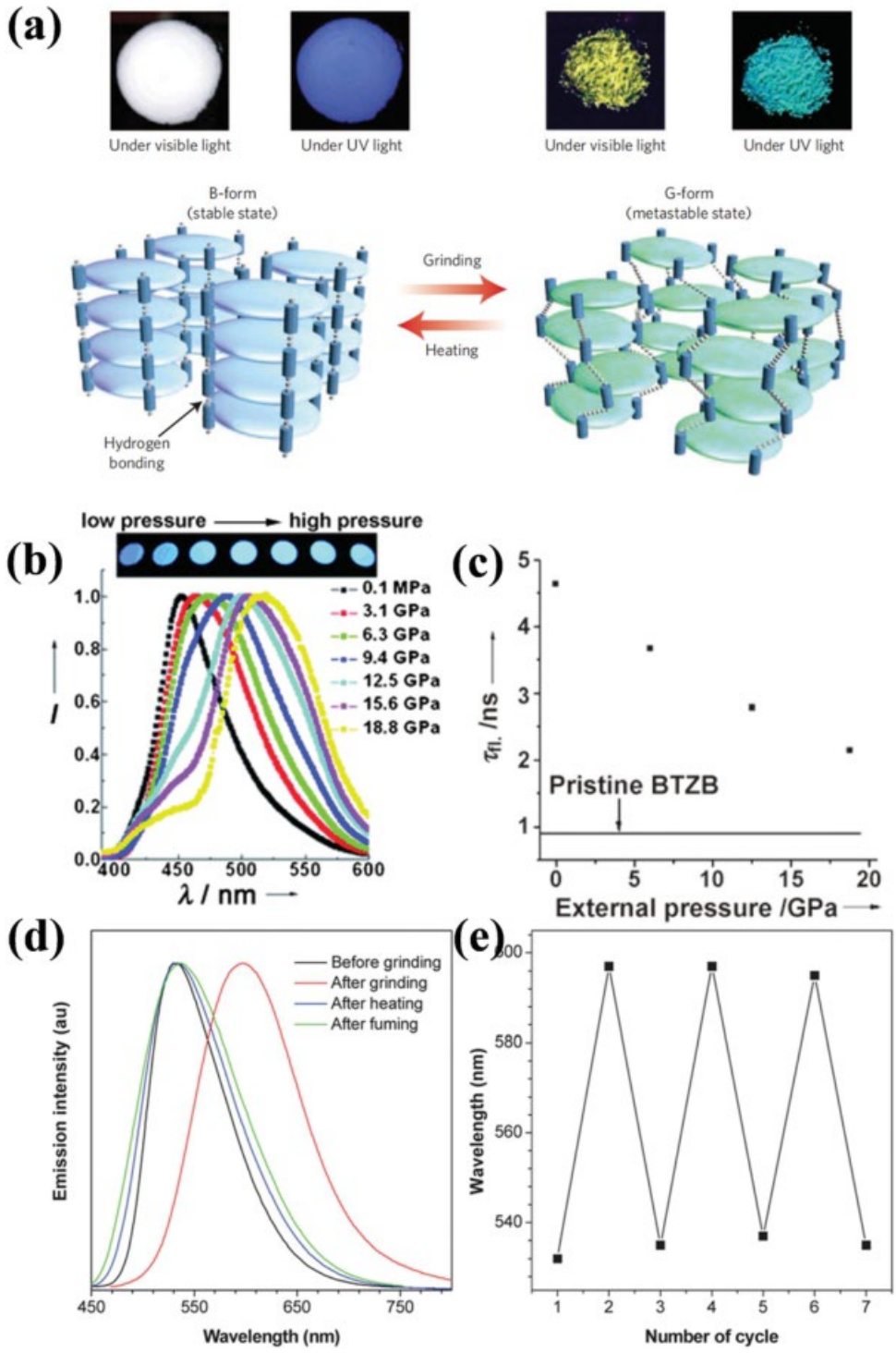

Figure 18. Tuning the luminescence of stimuli-responsive polymers. a) The photographs and mechanism of mechanically induced tuning of the luminescence in a pyrene-based compound. Reproduced with permission.[206] Copyright 2009, Nature Publishing Group. b) The emission spectra of BTZB/Mg_2Al-LDH samples under different pressures. The inset shows photographs of the samples. c) The emission lifetime of BTZB/Mg_2Al-LDH samples under various pressures. Reproduced with permission.[207] Copyright 2011, John Wiley & Sons, Inc. d) The emission spectra of TPE-Py crystals with a grinding–fuming/heating process. e) The solid-state emission peak of TPE-Py under repeated grinding and fuming/heating cycles. Reproduced with permission.[208] Copyright 2013, The Royal Society of Chemistry.

Sagara and Kato[206] reported mechanically induced tuning of the luminescence in a pyrene-based compound (**Figure 18**a). When pressing the white B-form with a spatula, the pyrene-based compound changes to a yellow G-form that presents a green emission, and then it can reverse to the B-form with heating. The tunable emission colour can be understood

by the change of twisting angles between pyrene units and the phenyl rings, and/or the inhibition of H-aggregation in the molecular assemblies.

Pressure, as one of the most common physical stimuli, should be a possible way to tune the luminescence of some luminescent polymers. An interesting example of pressure-induced emission modulation has been reported by Yan et al.[207] Prior to compression, the prepared BTZB/Mg_2Al-LDH samples exhibit a blue emission with the emission peak at 452 nm. After compression of the samples for 15 min at various pressures, a remarkable luminescence shift occurs, with a simultaneous broadening of the PL band (Figure 18b). Specifically, increasing the pressure from 0.1 MPa to 18.8 GPa, redshifts the emission peak from 452 to 515 nm. Meanwhile, the FWHM of the PL band exhibits a remarkable increase from 56 nm (0.1 MPa) to 95 nm (18.8 GPa). The emission colour change of compressed pellet samples can be readily observed by the naked eye (Figure 18b, inset). The redshift is caused by *J*-type aggregation in the interlayer galleries in layered double hydroxide (LDH). The emission lifetime (Figure 18c) of the compressed samples decreases from 4.63 ns (0.1 MPa) to 2.14 ns (18.8 GPa), further confirming the aggregation of the active centers. Interestingly, when the compressed sample was ground into a powder, after heating at 100 °C for 3 min, the emission peak is capable of reverting to the original wavelength (452 nm). Therefore, the emission can be modulated in a reversible manner, through applying pressure to the piezochromic materials.

Since the crystalline and amorphous aggregates of AIE phosphors present different luminescence properties, it is interesting to control the emission by phase modulation, induced by stress or heating. Tang's group synthesized a heteroatom-containing luminogen (TPE-Py) and investigated the luminescence behavior of the AIE phosphors with grinding/heating processes.[208] Under UV irradiation, the TPE-Py crystals exhibit an intense green emission at 515 nm. After gently grinding the green crystals with a metal spatula, orange powders are produced. The formed powders give an orange emission at 600 nm, leading to a large redshift of H85 nm (Figure 18d). In addition, through fuming powders with acetone vapor, the emission transformation is reversible. The conversion between the green and orange phosphors, as well as their corresponding PL spectra, can be repeated many times due to the nondestructive nature of the process (Figure 18e). The X-ray diffraction (XRD) patterns of these phosphors indicate that the phase of the as-prepared samples before grinding is crystalline, and that the ground sample is amorphous or slightly crystalline, whereas the thermally treated or fumed sample shows different crystalline peaks. It provides evidence that the emission modulation of TPE-Py originates from the phase change.

6.2. Temperature-Induced Tuning

Some experimental results reported by Jiang's group[209] show reversible tuning of the emission of responsive luminescent polymers through temperature. They fabricated a novel responsive phosphor $[Cu_8I_8(4\text{-dpda})_6]_n$ through combining organic ligands 4-dpda and inorganic Cu_8I_8. Then, the temperature-dependent PL of the prepared sample was investigated. As shown in **Figure 19**a, the sample gives a green emission with a peak at 530 nm (low-energy emission (LE)), at room temperature. When the temperature decreases to 170 K, a new emission band appears at 460 nm (high-energy emission (HE)). Further decreasing the temperature to 10 K, the HE intensity gradually increases with the LE band decreasing, and a slight blueshift to 447 nm is shown. The green emission of the LE band recovers when the sample is gradually warmed up to room temperature, indicating a reversible process. Interestingly, the sample shows an obvious redshift of 100 nm when grinding the sample, indicating that the prepared compound is a multistimuli-responsive luminescent material. In addition, the emission band broadens after grinding. The luminescence of the ground powder can be reverted to the original green emission through treating it with ethanol drops and drying it. According to the XRD results of the prepared, ground, and recovered samples, a phase change is apparent. The prepared compound is in the crystalline state. After grinding, the regular structure is dislocated by pressure, inducing an arrangement displacement, and the molecules become disordered. This structural change leads to the redshift and the broadened width. When the ground sample is recovered, the reflection peaks are restored, indicating a reversion from the amorphous to the crystalline phase. Thus, the externally induced modulation of molecular packing modes and frontier molecular orbitals alows the luminescence tuning.

Differing from $[Cu_8I_8(4\text{-dpda})_6]_n$, Uchiyama and co-workers developed a novel kind of fluorescent polymeric thermometer (FPT), which can be diffused throughout a cell.[210] With increasing temperature, the PL intensity is gradually enhanced (Figure 19b), and the fluorescence lifetime also increases (Figure 19c). Based on the temperature-dependent luminescence, fluorescence images (Figure 19d) and fluorescence lifetime images (Figure 19e) of FPT in COS7 cells were obtained to present the temperature mapping. The optical microscopy images indicate that such thermometry can map temperature distributions in living cells with a spatial resolution of 200 nm and a temperature resolution of 0.18–0.58 °C.

The luminescence of AIE phosphors is also sensitive to temperature, due to the structural change. Tang's group reported a controllable emission from dimethylformamide (DMF)-induced 4-(2,5-diphenyl-1H-pyrrol-1-yl) benzoic acid (TPPA) crystals through controlling the temperature.[211] Under 350 nm excitation, DMF-induced TPPA crystals give a strong blue emission band at 430 nm. As shown in Figure 19b, the emission intensity is stable at room temperature, but slightly decreases when increasing the temperature from 50 to 80 °C. The minor decrease in PL intensity is attributed to the heat-enhanced molecular vibration, consumed by the energy nonradiatively. When the temperature exceeds 80 °C, the PL intensity drops dramatically. When the temperature is over 110 °C, the emission is almost completely quenched, presenting a 100-fold decrease compared to the sample at room temperature. The quenching effect can be observed by the naked eye, as shown in the inset of Figure 19b. Figure 19c plots the PL intensity as a function of temperature, from which an obvious interval of emission quenching from 70 to 100 °C is seen. As shown in the differential curve of Figure 19c, the quenching rate at 88.3 °C is maximal. It is suggested that the thermal volatilization of DMF arises when the temperature is over 85 °C.

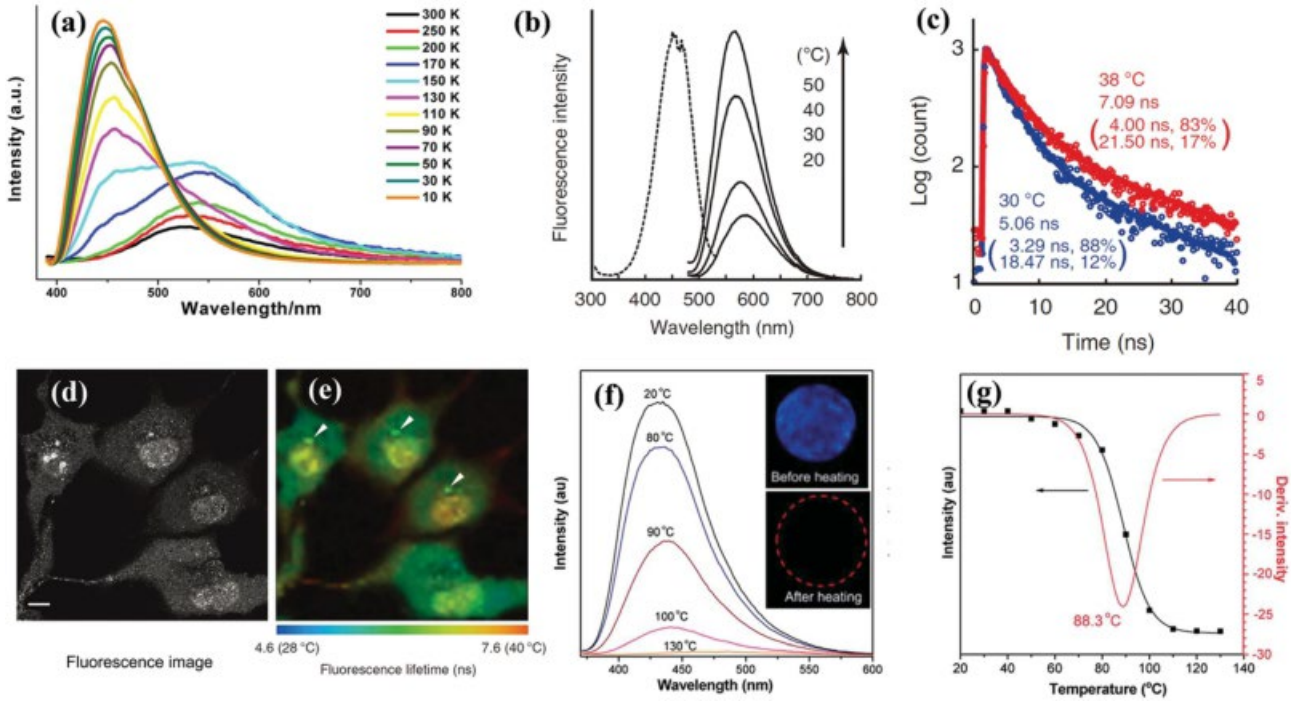

Figure 19. Tuning the luminescence of stimuli-responsive polymers. a) The temperature-dependent PL spectra of the as-prepared luminescent polymers. Reproduced with permission.[209] Copyright 2013, American Chemical Society. b) Temperature-dependent PL spectra in a cell. Left: Excitation band measured from the emission wavelength at 565 nm. Right: Emission spectra under 456-nm excitation. c) PL decay curves of FPT in a cell at 30 and 38 °C. d) Confocal fluorescence image of FPT in cells. e) Fluorescence lifetime image of FPT in cells. Reproduced with permission.[210] Copyright 2012, Nature Publishing Group. f) The emission spectra of the DMF-induced TPPA crystals under various temperatures. g) The PL intensity as a function of temperature. Black: The maximum emission intensity; red: its differential. Reproduced with permission.[211] Copyright 2013, The Royal Society of Chemistry.

In addition, UV light irradiation can be used to modulate the luminescence properties of organic phosphors. Park's group observed luminescent switching in stilbenic □-dimer crystals because of UV-induced isomerization.[212] With increasing UV irradiation time, the PL intensity of the prepared crystals is dramatically increased, resulting in a crystal quantum efficiency as high as 24%. The fluorescence enhancement could be considered a UV-induced lateral displacement of the luminescent molecular pairs. Subsequently, the fluorescence is absent after thermal annealing due to reverse displacement. According to this observation, such crystals should be useful for photochromic response applications.

7. Conclusions and Perspectives

Apart from conventional chemical ways, the luminescence of phosphors can be modulated by various physical methods. Specifically, the luminescence of Ln^{3+}-doped phosphors can be modified by various external fields, including electric or magnetic fields, mechanical stress, and temperature. The results to date indicate that the tunable luminescence of Ln^{3+}-doped phosphors by physical methods has striking and unusual features, which show the potential for various applications such as electro-optical modulators and magnetic-, temperature-, and stress-sensors. Plasmons, photons, and high-energy radiation can also alter the PL properties of Ln^{3+}-doped phosphors, allowing one to improve and optimize the performances of optical materials and devices by these alternative routes. Compared to Ln^{3+} ions, it is generally accepted that the electronic configuration of transition metal ions is more sensitive to their coordination environment. Therefore, the PL properties of transition metal ion-doped phosphors may be more responsive to external mechanical stress and temperature. In addition, the PL of main group metal ion-doped phosphors can be tuned by ultrashort-pulse lasers or high-energy radiation. For nanostructured semiconductors, including QDs, QWs, nanowires, and recently developed 2D-layered semiconductors, much research has focused on tuning the luminescence properties through electric fields and mechanical stress. In these studies, piezoelectric PMN-PT crystals have played a critical role in providing controllable biaxial strain to the phosphors. In stimuli-responsive luminescent polymers, stress and temperature can modify their luminescence. Because their colour changes can be readily detected, these polymers hold promise for practical applications such as security papers, mechanosensors, and indicators of mechanohistory. To expand this encouraging research field across a range of optical materials, some future development directions for tuning the luminescence of phosphors beyond chemical approaches are suggested.

In the majority of the aforementioned examples, one should note that, by physical stimuli, the tuning efficiency and scope of the luminescence are still restricted compared to the traditional chemical routes such as chemical substitution. Therefore, future investigations should focus on enhancing the effect of tuning the

luminescence, such as tuning the sensitivity and response speed to external stimuli. Alongside this, it is desirable to design and fabricate the phosphors capable of responding to multistimuli in a single system, which should be very helpful for multifunctional applications, such as electro-magneto-optical devices, multimode medical imaging agents, and so on. A multistimuli system based on a single compound can be realized by coupling different types of ions and classes of materials in nanostructured platforms.[213] For instance, Gd^{3+} and Mn^{2+} ions are known to demonstrate magnetic properties under magnetic fields. It is also noticeable that smart materials have fascinating properties that can be changed in a controlled fashion by external stimuli, such as mechanical stress, electric fields, and magnetic fields, as described above. Various multistimuli systems could be designed and fabricated by combining luminescent components with smart materials. Such a coupling could be considered one of the most promising ways to develop multistimuli luminescent systems. Our own group's previous works[51,87,151] seem to be just the tip of the iceberg for the subsequent development of these systems. In addition, it has been proven feasible to use atomically thin 2D materials, which should be more sensitive to external strain.[195] As a result, the combination of these materials may shed new light on yielding multifunctional devices. Apart from the material issues, the experimental methods and configurations suitable for characterizing the luminescence tuning via physical methods are still in their infancy, and far from optimal. The development of new experimental methods may be explored to combine microscopy and physical tuning techniques. For example, the joint system of spectrometry and microscopy (e.g., scanning probe microscopy, transmission electron microscopy) can be considered. Advanced characterization systems should be capable of simultaneously manipulating particles and measuring emission spectra of the luminescent samples under external stimuli at the nanoscale. Moreover, the investigations of fundamental mechanisms underlying the above-mentioned effects are still open issues. Further development depends on gaining comprehensive understandings of the fundamental physics and developing related theoretical models. Therefore, the development of physical models and simulations capable of predicting and interpreting the related phenomena are much needed. For example, the classical J–O theory is concisely given based on effective operators with a traditional form that has been utilized to illustrate the f spectra of Ln ions for many years.[214] The semiempirical approach of the J–O theory must be modified for tuning the luminescence of phosphors. Moreover, theoretical calculations based on first principles density functional theory (DFT) may be expanded to serve complex luminescent systems beyond phosphors for LEDs.[215] The development of integrated devices with tunable luminescence should be a future trend, and the proposed strategies in this review article can be considered to enlarge the research area. We believe that tuning luminescence by physical methods has great potential in many areas of optical materials and devices.

Acknowledgements

This research was supported by the grants from Research Grants Council of Hong Kong (GRF No. PolyU 5005/13P), CAS/SAFEA International Partnership Program for Creative Research Teams and National Natural Science Foundation of China (No. 51272218).

[1] W. M. Yen, S. Shionoya, H. Yamamoto, *Phosphor Handbook* 2nd ed., CRC Press, Boca Raton, FL **2007**.

[2] G. Blasse, B. Grabmaier, *Luminescent Materials*Springer, Berlin **1994**.

[3] a) M. McCarthy, B. Liu, E. Donoghue, I. Kravchenko, D. Kim, F. So, A. Rinzler, *Science* **2011**, *332*, 570; b) C. L. Salter, R. M. Stevenson, I. Farrer, C. A. Nicoll, D. A. Ritchie, A. J. Shields, *Nature* **2010**, *465*, 594; c) F. Ponce, D. Bour, *Nature* **1997**, *386*, 351.

[4] a) K. Bourzac, *Nature* **2013**, *493*, 283; b) K. Ziemelis, *Nature* **1999**, *399*, 408; c) Z. C. Dong, X. L. Zhang, H. Y. Gao, Y. Luo, C. Zhang, L. G. Chen, R. Zhang, X. Tao, Y. Zhang, J. L. Yang, J. G. Hou, *Nat. Photon.* **2010**, *4*, 50.

[5] a) V. I. Klimov, A. A. Mikhailovsky, S. Xu, A. Malko, J. A. Hollingsworth, C. A. Leatherdale, H. J. Eisler, M. G. Bawendi, *Science* **2000**, *290*, 314; b) M. Dahan, S. Levi, C. Luccardini, P. Rostaing, B. Riveau, A. Triller, *Science* **2003**, *302*, 442.

[6] a) X. Huang, S. Han, W. Huang, X. Liu, *Chem. Soc. Rev.* **2013**, *42*, 173; b) Y. Liu, D. Tu, H. Zhu, E. Ma, X. Chen, *Nanoscale* **2013**, *5*, 1369; c) S. J. Zeng, M. K. Tsang, C. F. Chan, K. L. Wong, J. H. Hao, *Biomaterials* **2012**, *33*, 9232.

[7] a) A. M. Smith, H. W. Duan, A. M. Mohs, S. M. Nie, *Adv. Drug Delivery Rev.* **2008**, *60*, 1226; b) D. T. Tu, W. Zheng, Y. S. Liu, H. M. Zhu, X. Y. Chen, *Coord. Chem. Rev.* **2014**, *273*, 13; c) S. J. Zeng, M. K. Tsang, C. F. Chan, K. L. Wong, B. Fei, J. H. Hao, *Nanoscale* **2012**, *4*, 5118; d) W. W. Ye, M.-K. Tsang, X. Liu, M. Yang, J. Hao, *Small* **2014**, *10*, 2390.

[8] a) T. Nobeshima, M. Nakakomi, K. Nakamura, N. Kobayashi, *Adv. Opt. Mater.* **2013**, *1*, 144; b) M. Shang, C. Li, J. Lin. *Chem. Soc. Rev.* **2014**, *43*, 1372; c) D. Q. Chen, Y. S. Wang, M. C. Hong, *Nano Energy* **2012**, *1*, 73; d) C. Zhang, H. P. Zhou, L. Y. Liao, W. Feng, W. Sun, Z. X. Li, C. H. Xu, C. J. Fang, L. D. Sun, Y. W. Zhang, C. H. Yan, *Adv. Mater.* **2010**, *22*, 633.

[9] a) S. C. Erwin, L. J. Zu, M. I. Haftel, A. L. Efros, T. A. Kennedy, D. J. Norris, *Nature* **2005**, *436*, 91; b) X. G. Peng, L. Manna, W. D. Yang, J. Wickham, E. Scher, A. Kadavanich, A. P. Alivisatos, *Nature* **2000**, *404*, 59; c) T. D. Nguyen, C. T. Dinh, T. O. Do, *ACS Nano* **2010**, *4*, 2263; d) X. Teng, Y. Zhu, W. Wei, S. Wang, J. Huang, R. Naccache, W. Hu, A. I. Y. Tok, Y. Han, Q. Zhang, Q. Fan, W. Huang, J. A. Capobianco, L. Huang, *J. Am. Chem. Soc.* **2012**, *134*, 8340.

[10] a) D. T. Tu, Y. S. Liu, H. M. Zhu, R. F. Li, L. Q. Liu, X. Y. Chen, *Angew. Chem. Int. Ed.* **2013**, *52*, 1128; b) H. Zhong, Z. Bai, B. Zou, *J. Phys. Chem. Lett.* **2012**, *3*, 3167; c) A. Hazarika, A. Layek, S. De, A. Nag, S. Debnath, P. Mahadevan, A. Chowdhury, D. D. Sarma, *Phys. Rev. Lett.* **2013**, *110*, 267401; d) Z. L. Wang, Z. W. Quan, P. Y. Jia, C. K. Lin, Y. Luo, Y. Chen, J. Fang, W. Zhou, C. J. O'Connor, J. Lin, *Chem. Mater.* **2006**, *18*, 2030.

[11] Y. Zhang, J. Hao, *J. Mater. Chem. C* **2013**, *1*, 5607.

[12] a) Z. J. Gu, L. Yan, G. Tian, S. J. Li, Z. F. Chai, Y. L. Zhao, *Adv. Mater.* **2013**, *25*, 3758; b) S. J. Zeng, J. J. Xiao, Q. B. Yang, J. H. Hao, *J. Mater. Chem.* **2012**, *22*, 9870.

[13] a) H. T. Wong, F. Vetrone, R. Naccache, H. L. W. Chan, J. H. Hao, J. A. Capobianco, *J. Mater. Chem.* **2011**, *21*, 16589; b) G. Bai, L. Tao, K. Li, L. Hu, Y. H. Tsang, *J. Non-Cryst. Solids* **2013**, *361*, 13; c) Y. Zhang, J. H. Hao, *J. Appl. Phys.* **2013**, *113*, 184112.

[14] Y. Yang, Y. Li, C. Wang, C. Zhu, C. Lv, X. Ma, D. Yang, *Adv. Opt. Mater.* **2014**, *2*, 240.

[15] Y. Lu, J. Zhao, R. Zhang, Y. Liu, D. Liu, E. M. Goldys, X. Yang, P. Xi, A. Sunna, J. Lu, *Nat. Photon.* **2013**, *8*, 32.

[16] S. F. Zhou, N. Jiang, B. T. Wu, J. H. Hao, J. R. Qiu, *Adv. Funct. Mater.* **2009**, *19*, 2081.

[17] G. Bai, Y. Zhang, J. Hao, *J. Mater. Chem. C* **2014**, *2*, 4631.

[18] D. Mocatta, G. Cohen, J. Schattner, O. Millo, E. Rabani, U. Banin, *Science* **2011**, *332*, 77.

[19] a) X. H. Zhong, M. Y. Han, Z. L. Dong, T. J. White, W. Knoll, *J. Am. Chem. Soc.* **2003**, *125*, 8589; b) Y. C. Li, M. F. Ye, C. H. Yang, X. H. Li, Y. F. Li, *Adv. Funct. Mater.* **2005**, *15*, 433.

[20] Y. K. Liu, J. A. Zapien, Y. Y. Shan, C. Y. Geng, C. S. Lee, S. T. Lee, *Adv. Mater.* **2005**, *17*, 1372.

[21] Y. Shirasaki, G. J. Supran, M. G. Bawendi, V. Bulovic´, *Nat. Photon.* **2013**, *7*, 13.

[22] A. Köhler, J. S. Wilson, R. H. Friend, *Adv. Eng. Mater.* **2002**, *4*, 453.

[23] C. Tang, S. VanSlyke, C. Chen, *J. Appl. Phys.* **1989**, *65*, 3610.

[24] O. Bolton, K. Lee, H.-J. Kim, K. Y. Lin, J. Kim, *Nat. Chem.* **2011**, *3*, 205.

[25] X. Michalet, F. F. Pinaud, L. A. Bentolila, J. M. Tsay, S. Doose, J. J. Li, G. Sundaresan, A. M. Wu, S. S. Gambhir, S. Weiss, *Science* **2005**, *307*, 538.

[26] B. O. Dabbousi, J. Rodriguez-Viejo, F. V. Mikulec, J. R. Heine, H. Mattoussi, R. Ober, K. F. Jensen, M. G. Bawendi, *J. Phys. Chem. B* **1997**, *101*, 9463.

[27] M. Y. Han, X. H. Gao, J. Z. Su, S. Nie, *Nat. Biotechnol.* **2001**, *19*, 631.

[28] X. Michalet, F. F. Pinaud, L. A. Bentolila, J. M. Tsay, S. Doose, J. J. Li, G. Sundaresan, A. M. Wu, S. S. Gambhir, S. Weiss, *Science* **2005**, *307*, 538.

[29] F. Wang, J. Wang, X. Liu, *Angew. Chem. Int. Ed.* **2010**, *49*, 7456.

[30] a) X. Ye, J. E. Collins, Y. Kang, J. Chen, D. T. N. Chen, A. G. Yodh, C. B. Murray, *Proc. Natl. Acad. Sci. USA* **2010**, *107*, 22430; b) H. Mai, Y. Zhang, L.-D. Sun, C.-H. Yan, *J. Phys. Chem. C* **2007**, *111*, 13721; c) X. Bai, H. Song, G. Pan, Y. Lei, T. Wang, X. Ren, S. Lu, B. Dong, Q. Dai, L. Fan, *J. Phys. Chem. C* **2007**, *111*, 13611; d) H. Song, B. Sun, T. Wang, S. Lu, L. Yang, B. Chen, X. Wang, X. Kong, *Solid State Commun.* **2004**, *132*, 409.

[31] G. Yi, G. Chow, *Chem. Mater.* **2007**, *298*, 341.

[32] F. Wang, R. Deng, J. Wang, Q. Wang, Y. Han, H. Zhu, X. Chen, X. Liu, *Nat. Mater.* **2011**, *10*, 968.

[33] Y. Zhang, T.-H. Wang, *Theranostics* **2012**, *2*, 631.

[34] H. Mattoussi, J. M. Mauro, E. R. Goldman, G. P. Anderson, V. C. Sundar, F. V. Mikulec, M. G. Bawendi, *J. Am. Chem. Soc.* **2000**, *122*, 12142.

[35] P. Reiss, J. Bleuse, A. Pron, *Nano Lett.* **2002**, *2*, 781.

[36] J. J. Li, Y. A. Wang, W. Z. Guo, J. C. Keay, T. D. Mishima, M. B. Johnson, X. G. Peng, *J. Am. Chem. Soc.* **2003**, *125*, 12567.

[37] J. S. Steckel, J. P. Zimmer, S. Coe-Sullivan, N. E. Stott, V. Bulovic´, M. G. Bawendi, *Angew. Chem. Int. Ed.* **2004**, *43*, 2154.

[38] K. Ogata, E. Sutter, X. Zhu, S. Hofmann, *Nanotechnology* **2011**, *22*, 365305.

[39] M.-K. Tsang, S. Zeng, H. L. W. Chan, J. Hao, *Opt. Mater.* **2013**, *35*, 2691.

[40] W. Niu, S. Wu, S. Zhang, *J. Mater. Chem.* **2010**, *20*, 9113.

[41] M. C. Tan, L. Al-Baroudi, R. E. Riman, *ACS Appl. Mater. Interfaces* **2011**, *3*, 3910.

[42] C. Yan, A. Dadvand, F. Rosei, D. F. Perepichka, *J. Am. Chem. Soc.* **2010**, *132*, 8868.

[43] a) R. J. Warburton, C. Schäflein, D. Haft, F. Bickel, A. Lorke, K. Karrai, J. M. Garcia, W. Schoenfeld, P. M. Petroff, *Nature* **2000**, *405*, 926; b) J. R. Jain, A. Hryciw, T. M. Baer, D. A. B. Miller, M. L. Brongersma, R. T. Howe, *Nat. Photon.* **2012**, *6*, 398; c) Q. X. Zhao, H. Weman, B. Monemar, *J. Lumin.* **1988**, *40*, 151.

[44] S. H. Autler, C. Townes, *Phys. Rev.* **1955**, *100*, 703.

[45] a) T. Takeuchi, S. Sota, M. Katsuragawa, M. Komori, H. Takeuchi, H. Amano, I. Akasaki, *Jpn. J. Appl. Phys. Part 2-Lett.* **1997**, *36*, L382; b) M. Leroux, N. Grandjean, M. Laugt, J. Massies, B. Gil, P. Lefebvre, P. Bigenwald, *Phys. Rev. B* **1998**, *58*, 13371.

[46] S. Wu, W. Xia, *J. Appl. Phys.* **2013**, *114*, 043709.

[47] S. Empedocles, M. Bawendi, *Science* **1997**, *278*, 2114.

[48] a) U. Jahn, S. Dhar, M. Ramsteiner, K. Fujiwara, *Phys. Status Solidi A* **2004**, *201*, 2619; b) J. P. Evans, V. Saxena, H. P. Hughes, *Phys. Status Solidi B* **1997**, *204*, 125.

[49] a) B. R. Judd, *Phys. Rev.* **1962**, *197*, 750; b) G. S. Ofelt, *J. Chem. Phys.* **1962**, *37*, 511.

[50] O. L. Malta, L. D. Carlos, *Quim. Nova* **2003**, *26*, 889.

[51] J. H. Hao, Y. Zhang, X. H. Wei, *Angew. Chem. Int. Ed.* **2011**, *50*, 6876.

[52] R. Korlacki, R. F. Saraf, S. Ducharme, *Appl. Phys. Lett.* **2011**, *99*, 153112.

[53] a) Y. Fan, M. Bauer, L. Kador, K. Allakhverdiev, E. Y. Salaev, *J. Appl. Phys.* **2002**, *91*, 1081; b) E. Rothenberg, M. Kazes, E. Shaviv, U. Banin, *Nano Lett.* **2005**, *5*, 1581.

[54] D. M. Adams, J. Kerimo, C. Y. Liu, A. J. Bard, P. F. Barbara, *J. Phys. Chem. B* **2000**, *104*, 6728.

[55] H. Ebert, *Rep. Prog. Phys.* **1996**, *59*, 1665.

[56] Y. Liu, D. Wang, J. Shi, Q. Peng, Y. Li, *Angew. Chem. Int. Ed.* **2013**, *52*, 4366.

[57] M. Hayne, B. Bansal, *Luminescence* **2012**, *27*, 179.

[58] a) M. V. Yakushev, Y. Feofanov, R. W. Martin, R. D. Tomlinson, a. V. Mudryi, *J. Phys. Chem. Solids* **2003**, *64*, 2011; b) a. Polimeni, S. T. Stoddart, M. Henini, L. Eaves, P. C. Main, K. Uchida, R. K. Hayden, N. Miura, *Phys. E* **1998**, *2*, 662; c) S. Raymond, S. Studenikin, S. J. Cheng, M. Pioro-Ladrière, M. Ciorga, P. J. Poole, M. D. Robertson, *Semicond. Sci. Technol.* **2003**, *18*, 385.

[59] B. Hu, L. Yan, M. Shao, *Adv. Mater.* **2009**, *21*, 1500.

[60] Z.-W. Ma, J.-P. Zhang, X. Wang, Y. Yu, J.-B. Han, G.-H. Du, L. Li, *Opt. Lett.* **2013**, *38*, 3754.

[61] S. K. Ghosh, T. Pal, *Chem. Rev.* **2007**, *107*, 4797.

[62] S. Zeng, K.-T. Yong, I. Roy, X.-Q. Dinh, X. Yu, F. Luan, *Plasmonics* **2011**, *6*, 491.

[63] B.-K. Vlasta, F. Piercarlo, K. Jaroslav, *Chem. Rev.* **1991**, *91*, 1035.

[64] a) G. Armelles, A. Cebollada, A. García-Martín, M. U. González, *Adv. Opt. Mater.* **2013**, *1*, 10; b) C. C. Lu, X. Y. Hu, H. Yang, Q. H. Gong, *Adv. Opt. Mater.* **2013**, *1*, 792; c) Y. Zhu, X. Hu, Y. Huang, H. Yang, Q. H. Gong, *Adv. Opt. Mater.* **2013**, *1*, 61; d) Y. D. Zhao, X. Liu, D. Y. Lei, Y. Chai, *Nanoscale* **2014**, *6*, 1311.

[65] J. Goffard, D. Gérard, P. Miska, A.-L. Baudrion, R. Deturche, J. Plain, *Sci. Rep.* **2013**, *3*, 2672.

[66] L. Zhao, T. Ming, H. J. Chen, Y. Liang, J. F. Wang, *Nanoscale* **2011**, *3*, 3849.

[67] a) Y. Lin, C. X. Xu, J. T. Li, G. Y. Zhu, X. Y. Xu, J. Dai, B. P. Wang, *Adv. Opt. Mater.* **2013**, *1*, 940; b) J. S. Biteen, N. S. Lewis, H. A. Atwater, H. Mertens, A. Polman, *Appl. Phys. Lett.* **2006**, *88*, 131109; c) M. Eichelbaum, K. Rademann, *Adv. Funct. Mater.* **2009**, *19*, 2045.

[68] D. Dai, Z. Dong, J. Fan, *Nanotechnology* **2013**, *24*, 025201.

[69] K. Okamoto, I. Niki, A. Shvartser, Y. Narukawa, T. Mukai, A. Scherer, *Nat. Mater.* **2004**, *3*, 601.

[70] J. R. Qiu, X. W. Jiang, C. S. Zhu, M. Shirai, J. Si, N. Jiang, K. Hirao, *Angew. Chem. Int. Ed.* **2004**, *43*, 2230.

[71] J. R. Qiu, *Chem. Rec.* **2004**, *4*, 50.

[72] J. R. Qiu, *J. Ceram. Soc. Jpn.* **2001**, *109*, S25.

[73] S. F. Zhou, W. Q. Lei, N. Jiang, J. H. Hao, E. Wu, H. P. Zeng, J. R. Qiu, *J. Mater. Chem.* **2009**, *19*, 4603.

[74] S. F. Zhou, N. Jiang, K. Miura, S. Tanabe, M. Shimizu, M. Sakakura, Y. Shimotsuma, M. Nishi, J. R. Qiu, K. Hirao, *J. Am. Chem. Soc.* **2010**, *132*, 17945.

[75] J. Choi, N. S. Wang, V. Reipa, *Langmuir* **2007**, *23*, 3388.
[76] H. Koyama, N. Koshida, *J. Appl. Phys.* **1993**, *74*, 6365.
[77] A. B. Cruz, Q. Shen, T. Toyoda, *Mater. Sci. Eng. C* **2005**, *25*, 761.
[78] Y. L. Huang, W. X. Zhao, L. Shi, H. J. Seo, *J. Alloy Compd.* **2009**, *477*, 936.
[79] a) H. Scheel, C. Zollfrank, P. Greil, *J. Mater. Res.* **2009**, *24*, 1709; b) C. Dotzler, G. V. M. Williams, A. Edgar, S. Schweizer, B. Henke, J. M. Spaeth, A. Bittar, J. Hamlin, C. Dunford, *J. Appl. Phys.* **2006**, *100*, 033102.
[80] Z. L. Wang, *Nano Today* **2010**, *5*, 540.
[81] a) Y. Zhang, Y. Yang, Z. L. Wang, *Energy Environ. Sci.* **2012**, *5*, 6850; b) C. F. Pan, S. M. Niu, Y. Ding, L. Dong, R. M. Yu, Y. Liu, G. Zhu, Z. L. Wang, *Nano Lett.* **2012**, *12*, 3302; c) X. N. Wen, W. Z. Wu, Z. L. Wang, *Nano Energy* **2013**, *2*, 1093.
[82] J. C. Zhang, C. N. Xu, S. Kamimura, Y. Terasawa, H. Yamada, X. S. Wang, *Opt. Express* **2013**, *21*, 12976.
[83] Z. G. Sheng, J. Gao, Y. P. Sun, *Phys. Rev. B* **2009**, *79*, 174437.
[84] Z. P. Wu, L. Wang, E. J. Guo, J. Gao, *J. Appl. Phys.* **2012**, *111*, 07E105.
[85] N. Yasuda, N. Hidayah, H. Ohwa, Y. Tachi, Y. Yamashita, I. J. Hlinka, M. Iwata, H. Terauchi, Y. Ishibashi, *J. Phys. Soc. Jpn.* **2013**, *82*, 173.
[86] R. Trotta, P. Atkinson, J. Plumhof, E. Zallo, R. Rezaev, S. Kumar, S. Baunack, J. Schroeter, A. Rastelli, O. Schmidt, *Adv. Mater.* **2012**, *24*, 2668.
[87] G. Bai, Y. Zhang, J. Hao, *Sci. Rep.* **2014**, *4*, 5724.
[88] G. Signorello, S. Karg, M. T. Bjork, B. Gotsmann, H. Riel, *Nano Lett.* **2013**, *13*, 917.
[89] Y. F. Hu, Y. Zhang, L. Lin, Y. Ding, G. Zhu, Z. L. Wang, *Nano Lett.* **2012**, *12*, 3851.
[90] N. Komiya, T. Muraoka, M. Iida, M. Miyanaga, K. Takahashi, T. Naota, *J. Am. Chem. Soc.* **2011**, *133*, 16054.
[91] E.-H. Song, S. Ding, M. Wu, S. Ye, F. Xiao, G.-P. Dong, Q.-Y. Zhang, *J. Mater. Chem. C* **2013**, *1*, 4209.
[92] D. Wawrzynczyk, A. Bednarkiewicz, M. Nyk, W. Strek, M. Samoc, *Nanoscale* **2012**, *4*, 6959.
[93] a) C. D. Brites, P. P. Lima, N. J. Silva, A. Millán, V. S. Amaral, F. Palacio, L. D. Carlos, *Nanoscale* **2012**, *4*, 4799; b) F. Vetrone, R. Naccache, A. Zamarrón, A. Fuente, F. Sanz-Rodríguez, L. Maestro, E. Rodriguez, D. Jaque, J. Solé, J. Capobianco, *ACS Nano* **2010**, *4*, 3254; c) B. Dong, B. Cao, Y. He, Z. Liu, Z. Li, Z. Feng, *Adv. Mater.* **2012**, *24*, 1987.
[94] K. Wu, J. Cui, X. Kong, Y. Wang, *J. Appl. Phys.* **2011**, *110*, 053510.
[95] M. Shinn, W. Sibley, M. Drexhage, R. Brown, *Phys. Rev. B* **1983**, *27*, 6635.
[96] P. Santos, E. Gouveia, M. Araujo, A. Gouveia-Neto, A. Sombra, J. Neto, *Appl. Phys. Lett.* **1999**, *74*, 3607.
[97] a) T.-C. Liu, Z.-L. Huang, H.-Q. Wang, J.-H. Wang, X.-Q. Li, Y.-D. Zhao, Q.-M. Luo, *Anal. Chem. Acta* **2006**, *559*, 120; b) O. Schöps, N. Le Thomas, U. Woggon, M. V. Artemyev, *J. Phys. Chem. B* **2006**, *110*, 2074.
[98] a) G. Ramírez-Flores, H. Navarro-Contreras, A. Lastras-Martínez, R. Powell, J. Greene, *Phys. Rev. B* **1994**, *50*, 8433; b) G. W. Walker, V. C. Sundar, C. M. Rudzinski, A. W. Wun, M. G. Bawendi, D. G. Nocera, *Appl. Phys. Lett.* **2003**, *83*, 3555; c) D. Valerini, A. Cretí, M. Lomascolo, L. Manna, R. Cingolani, M. Anni, *Phys. Rev. B* **2005**, *71*, 235409.
[99] Y. P. Varshni, *Physica* **1967**, *34*, 149.
[100] P. Chin, C. Donega, S. Bavel, S. Meskers, N. Sommerdijk, R. Janssen, *J. Am. Chem. Soc.* **2007**, *129*, 14880.
[101] Z. Gong, S. Zhen, F. Wu, L. Zhe, *Chin. Phys. Lett.* **2002**, *19*, 578.
[102] G. Y. Zhong, X. M. Ding, J. Zhou, N. Jiang, W. Huang, X. Y. Hou, *Chem. Phys. Lett.* **2006**, *420*, 347.
[103] H. Bassler, B. Schweitzer, *Acc. Chem. Res.* **1999**, *32*, 173.
[104] L. Vina, S. Logothetidis, M. Cardona, *Phys. Rev. B* **1984**, *30*, 1979.
[105] a) V. D. Rodriguez, V. K. Tikhomirov, J. J. Velazquez, M. V. Shestakov, V. V. Moshchalkov, *Adv. Opt. Mater.* **2013**, *1*, 747; b) G. Bai, L. Tao, K. Li, L. Hu, Y. H. Tsang, *Opt. Mater.* **2013**, *35*, 1247; c) K. Li, Q. Zhang, G. Bai, S. Fan, J. Zhang, L. Hu, *J. Alloys Compd.* **2010**, *504*, 573.
[106] Y. H. Tsang, D. J. Binks, B. D. O. Richards, A. Jha, *Laser Phys. Lett.* **2011**, *8*, 729.
[107] W. Z. Lv, Y. C. Jia, Q. Zhao, M. M. Jiao, B. Q. Shao, W. Lu, H. P. You, *Adv. Opt. Mater.* **2014**, *2*, 183.
[108] a) E. Song, S. Ding, M. Wu, S. Ye, F. Xiao, S. Zhou, Q. Zhang, *Adv. Opt. Mater.* **2014**, *2*, 670; b) Y. Ding, J. Gu, T. Zhang, A.-X. Yin, L. Yang, Y.-W. Zhang, C.-H. Yan, *J. Am. Chem. Soc.* **2012**, *134*, 3255; c) B. Zhou, L. Tao, Y. H. Tsang, W. Jin, *J. Mater. Chem. C* **2013**, *1*, 4313.
[109] a) H. Zhou, X. M. Chen, G. H. Wu, F. Gao, N. Qin, D. H. Bao, *J. Am. Chem. Soc.* **2010**, *132*, 1790; b) J. Hao, Z. Lou, I. Renaud, M. Cocivera, *Thin Solid Films* **2004**, *467*, 182; c) J. H. Hao, J. Gao, M. Cocivera, *Appl. Phys. Lett.* **2003**, *82*, 2224.
[110] R. Boyn, *Phys. Status Solidi B* **1988**, *148*, 11.
[111] J. Bunzli, S. Comby, A. Chauvin, C. Vandevyver, *J. Rare Earth* **2007**, *25*, 257.
[112] S. Faulkner, S. J. A. Pope, B. P. Burton-Pye, *Appl. Spectrosc. Rev.* **2005**, *40*, 1.
[113] X. Tian, Z. Wu, Y. Jia, J. Chen, R. Zheng, Y. Zhang, H. Luo, *Appl. Phys. Lett.* **2013**, *102*, 042907.
[114] Q. Zhang, H. Sun, Y. Zhang, *J. Am. Ceram. Soc.* **2014**, *97*, 868.
[115] V. K. Tikhomirov, L. F. Chibotaru, D. Saurel, P. Gredin, M. Mortier, V. V. Moshchalkov, *Nano Lett.* **2009**, *9*, 721.
[116] S. K. Singh, K. Kumar, M. K. Srivastava, D. K. Rai, S. B. Rai, *Opt. Lett.* **2010**, *35*, 1575.
[117] S. Schietinger, T. Aichele, H.-Q. Wang, T. Nann, O. Benson, *Nano Lett.* **2010**, *10*, 134.
[118] H. Zhang, Y. Li, I. A. Ivanov, Y. Qu, Y. Huang, X. Duan, *Angew. Chem. Int. Ed.* **2010**, *122*, 2927.
[119] P. Yuan, Y. H. Lee, M. K. Gnanasammandhan, Z. Guan, Y. Zhang, Q.-H. Xu, *Nanoscale* **2012**, *4*, 5132.
[120] S. Saboktakin, X. Ye, S. J. Oh, S.-H. Hong, A. T. Fafarman, U. K. Chettiar, N. Engheta, C. B. Murray, C. R. Kagan, *ACS Nano* **2012**, *6*, 8758.
[121] W. Zhang, F. Ding, S. Y. Chou, *Adv. Mater.* **2012**, *24*, OP236.
[122] a) J. H. Hao, M. Cocivera, *Appl. Phys. Lett.* **2001**, *79*, 740; b) J. H. Hao, M. Cocivera, *Appl. Phys. Lett.* **2002**, *81*, 4154; c) J. H. Hao, J. Gao, *Appl. Phys. Lett.* **2004**, *85*, 3720.
[123] A. B. Yusov, V. P. Shilov, *Russ. Chem. Bull. Int. Ed.* **2000**, *49*, 1925.
[124] a) J. R. Qiu, K. Kojima, K. Miura, T. Mitsuyu, K. Hirao, *Opt. Lett.* **1999**, *24*, 786; b) G. J. Park, T. Hayakawa, M. Nogami, *J. Phys.: Condens. Matter* **2003**, *15*, 1259.
[125] M. Kusaba, N. Nakashima, W. Kawamura, Y. Izawa, C. Yamanaka, *Chem. Phys. Lett.* **1992**, *197*, 136.
[126] N. Nobuaki, S. Nakamura, S. Sakabe, H. Schillinger, Y. Hamanaka, C. Yamanaka, M. Kusaba, N. Ishihara, Y. Izawa, *J. Phys. Chem. A* **1999**, *103*, 3910.
[127] J. Qiu, K. Miura, T. Suzuki, T. Mitsuyu, K. Hirao, *Appl. Phys. Lett.* **1999**, *74*, 10.
[128] D. Nishida, M. Kusaba, T. Yatsuhashi, N. Nakashima, *Chem. Phys. Lett.* **2008**, *465*, 238.
[129] Y. Huang, C. Jiang, K. Jang, H. S. Lee, E. Cho, M. Jayasimhadri, S.-S. Yi, *J. Appl. Phys.* **2008**, *103*, 113519.
[130] D. Sun, J. Luo, Q. Zhang, J. Xiao, J. Xu, H. Jiang, S. Yin, *J. Lumin.* **2008**, *128*, 1886.
[131] Y. Huang, W. Zhao, L. Shi, H. J. Seo, *J. Alloys Compd.* **2009**, *477*, 936.
[132] C. Zhu, Y. Yang, G. Chen, S. Baccaro, A. Cecilia, M. Falconieri, *J. Phys. Chem. Solids* **2007**, *68*, 1721.

[133] R. Valiente, M. Millot, F. Rodríguez, J. González, J. M. Broto, S. George, S. García-Revilla, Y. Romanyuk, M. Pollnau, *High Pressure Res.* **2009**, *29*, 748.

[134] C. R. Lecuna, R. M. Rodríguez, R. Valiente, J. González, F. Rodríguez, K. W. Krämer, H. U. Güdel, *Chem. Mater.* **2011**, *23*, 3442.

[135] C. Bungenstock, T. Tröster, W. B. Holzapfel, R. Bini, L. Ulivi, S. Cavalieri, *J. Phys.: Condens. Matter* **1998**, *10*, 9329.

[136] R. Turos-Matysiak, H. R. Zheng, J. W. Wang, W. M. Yen, R. S. Meltzer, T. Łukasiewicz, M. wirkowicz, M. Grinberg, *J. Lumin.* **2007**, *122*, 322.

[137] a) X. Wang, C. N. Xu, H. Yamada, K. Nishikubo, X. G. Zheng, *Adv. Mater.* **2005**, *17*, 1254; b) S. Kamimura, H. Yamada, C. N. Xu, *Appl. Phys. Lett.* **2012**, *101*, 091113; c) J. Botterman, K. V. Eeckhout, I. D. Baere, D. Poelman, P. F. Smet, *Acta Mater.* **2012**, *60*, 5494.

[138] J. C. Zhang, C. N. Xu, Y. Z. Long, *Opt. Express* **2013**, *21*, 13699.

[139] A. M. Pires, O. A. Serra, S. Heer, H. U. Güdel, *J. Appl. Phys.* **2005**, *98*, 063529.

[140] P. V. dos Santos, M. T. de Araujo, A. S. Gouveia-Neto, J. A. M. Neto, A. S. B. Sombra, *Appl. Phys. Lett.* **1998**, *73*, 578.

[141] C. D. Brites, P. P. Lima, N. J. Silva, A. Millán, V. S. Amaral, F. Palacio, L. D. Carlos, *Adv. Mater.* **2010**, *22*, 4499.

[142] J. Dong, J. I. Zink, *ACS Nano* **2014**, *8*, 5199.

[143] a) M. T. Carlson, A. Khan, H. H. Richardson, *Nano Lett.* **2011**, *11*, 1061; b) M. L. Debasu, D. Ananias, I. Pastoriza-Santos, L. M. Liz-Marzán, J. Rocha, L. D. Carlos, *Adv. Mater.* **2013**, *25*, 4868.

[144] K. K. -W. Lo, A. W. -T. Choi, W. H. -T. Law, *Dalton Trans.* **2012**, *41*, 6021.

[145] Y. Chi, P.-T. Chou, *Chem. Soc. Rev.* **2010**, *39*, 638.

[146] a) J. Yu, H. Liu, Y. Wang, F. Fernandez, W. Jia, L. Sun, C. Jin, D. Li, J. Liu, S. Huang, *Opt. Lett.* **1997**, *22*, 913; b) D. Gallagher, W. Heady, J. Racz, R. Bhargava, *J. Mater. Res.* **1995**, *10*, 870.

[147] A. A. Bol, A. Meijerink, *J. Phys. Chem. B* **2001**, *105*, 10203.

[148] D.-R. Jung, J. Kim, B. Park, *Appl. Phys. Lett.* **2010**, *96*, 211908.

[149] R. A. Forman, S. Block, J. Piermari, J. D. Barnett, S. Block, *Science* **1972**, *176*, 284.

[150] O. S. Wenger, G. M. Salley, H. U. Gudel, *J. Phys. Chem. B* **2002**, *106*, 10082.

[151] Y. Zhang, G. Gao, H. L. W. Chan, J. Dai, Y. Wang, J. Hao, *Adv. Mater.* **2012**, *24*, 1729.

[152] G. Gao, M. Peng, L. Wondraczek, *Opt. Lett.* **2012**, *37*, 1166.

[153] T. Suzuki, G. S. Murugan, Y. Ohishi, *Appl. Phys. Lett.* **2005**, *86*, 131903.

[154] J. Xu, L. B. Su, *J. Inorg. Mater.* **2011**, *26*, 347.

[155] M. Y. Sharonov, A. B. Bykov, V. Petricevic, R. R. Alfano, *Opt. Lett.* **2008**, *33*, 2131.

[156] B. B. Xu, J. H. Hao, Q. B. Guo, J. C. Wang, G. X. Bai, B. Fei, S. F. Zhou, J. R. Qiu, *J. Mater. Chem. C* **2014**, *2*, 2482.

[157] I. A. Bufetov, M. A. Melkumov, S. V. Firstov, A. V. Shubin, S. L. Semenov, V. V. Vel'miskin, A. E. Levchenko, E. G. Firstova, E. M. Dianov, *Opt. Lett.* **2011**, *36*, 166.

[158] M. Y. Peng, G. P. Dong, L. Wondraczek, L. L. Zhang, N. Zhang, J. R. Qiu, *J. Non-Cryst. Solids* **2011**, *357*, 2241.

[159] M. Y. Peng, Q. Z. Zhao, J. R. Qiu, L. Wondraczek, *J. Am. Ceram. Soc.* **2009**, *92*, 542.

[160] L. Su, J. Yu, P. Zhou, H. Li, L. Zheng, Y. Yang, F. Wu, H. Xia, J. Xu, *Opt. Lett.* **2009**, *34*, 2504.

[161] B. B. Xu, D. Z. Tan, M. J. Guan, Y. Teng, J. J. Zhou, J. R. Qiu, Z. L. Hong, *J. Electrochem. Soc.* **2011**, *158*, G203.

[162] L. I. Gurinovich, A. A. Lutich, A. P. Stupak, S. Y. Prislopsky, E. K. Rusakov, M. V. Artemyev, S. V. Gaponenko, H. V. Demir, *Semiconductors* **2009**, *43*, 1008.

[163] a) U. Hakanson, H. Hakanson, M. K. J. Johansson, L. Samuelson, M. E. Pistol, *J. Vac. Sci. Technol. B* **2003**, *21*, 2344; b) A. Gonzalez, E. Menendez-Proupin, *Phys. E* **2000**, *8*, 333.

[164] D. Y. Lei, J. Li, H. C. Ong, *Appl. Phys. Lett.* **2007**, *91*, 021112.

[165] P. J. Simmonds, C. D. Yerino, M. Sun, B. L. Liang, D. L. Huffaker, V. G. Dorogan, Y. Mazur, G. Salamo, M. L. Lee, *ACS Nano* **2013**, *7*, 5017.

[166] a) D. Bera, L. Qian, T. K. Tseng, P. H. Holloway, *Materials* **2010**, *3*, 2260; b) L. Tang, R. Ji, X. Li, G. Bai, C. P. Liu, J. Hao, J. Lin, H. Jiang, K. S. Teng, Z. Yang, *ACS Nano* **2014**, *8*, 6312.

[167] a) Y. Yin, A. P. Alivisatos, *Nature* **2005**, *437*, 664; b) T. Trindade, P. O'Brien, N. L. Pickett, *Chem. Mater.* **2001**, *13*, 3843.

[168] a) E. S. Moskalenko, M. Larsson, K. F. Karlsson, P. O. Holtz, B. Monemar, W. V. Schoenfeld, P. M. Petroff, *Nano Lett.* **2007**, *7*, 188; b) D. F. Fang, R. Chen, H. W. Liu, Z. M. Zhang, Z. J. Ding, *J. Nanosci. Nanotechnol.* **2010**, *10*, 7600.

[169] P. Wojnar, J. Suffczynski, K. Kowalik, A. Golnik, G. Karczewski, J. Kossut, *Phys. Rev. B* **2007**, *75*, 155301.

[170] P. Wojnar, G. Karczewski, J. Suffczynski, M. Goryca, A. Golnik, K. Kowalik, J. Kossut, C. Wetzel, A. Khan, *Phys. Status Solidi C* **2011**, *8*, 8.

[171] H. Mertens, J. S. Biteen, H. A. Atwater, A. Polman, *Nano Lett.* **2006**, *6*, 2622.

[172] L. Hu, H. Wu, Z. Wan, C. Cai, T. Xu, T. Lou, B. Zhang, *New J. Phys.* **2012**, *14*, 013059.

[173] a) K. Jöns, R. Hafenbrak, R. Singh, F. Ding, J. Plumhof, A. Rastelli, O. Schmidt, G. Bester, P. Michler, *Phys. Rev. Lett.* **2011**, *107*, 217402; b) R. Trotta, E. Zallo, C. Ortix, P. Atkinson, J. Plumhof, J. Van den Brink, A. Rastelli, O. Schmidt, *Phys. Rev. Lett.* **2012**, *109*, 147401.

[174] O. Labeau, P. Tamarat, B. Lounis, *Phys. Rev. Lett.* **2003**, *90*, 257404.

[175] S. F. Wuister, A. van Houselt, C. D. M. Donega, D. Vanmaekelbergh, A. Meijerink, *Angew. Chem. Int. Ed.* **2004**, *43*, 3029.

[176] E. E. Mendez, G. Bastard, L. L. Chang, L. Esaki, H. Morkoc, R. Fischer, *Phys. B+C* **1983**, *117*, 711.

[177] D. Huang, S. Lyo, *Phys. Rev. B* **1999**, *59*, 7600.

[178] M. Orlita, R. Grill, P. Hlidek, M. Zvara, G. H. Dohler, S. Malzer, M. Byszewski, *Phys. Rev. B* **2005**, *72*, 113101.

[179] J. Yin, Y. Li, S. Chen, J. Li, J. Kang, W. Li, P. Jin, Y. Chen, Z. Wu, J. Dai, Y. Fang, C. Chen, *Adv. Opt. Mater.* **2014**, *2*, 451.

[180] M. Aumer, S. LeBoeuf, S. Bedair, M. Smith, J. Lin, H. Jiang, *Appl. Phys. Lett.* **2000**, *77*, 821.

[181] N. A. Shapiro, H. Feick, W. Hong, M. Cich, R. Armitage, E. R. Weber, *J. Appl. Phys.* **2003**, *94*, 4520.

[182] P. G. Eliseev, P. Perlin, J. Lee, M. Osin ski, *Appl. Phys. Lett.* **1997**, *71*, 569.

[183] Y.-H. Cho, G. H. Gainer, A. J. Fischer, J. J. Song, S. Keller, U. K. Mishra, S. P. DenBaars, *Appl. Phys. Lett.* **1998**, *73*, 1370.

[184] a) S. Mokkapati, D. Saxena, N. Jiang, P. Parkinson, J. Wong-Leung, Q. Gao, H. H. Tan, C. Jagadish, *Nano Lett.* **2012**, *12*, 6428; b) Z. L. Wang, R. S. Yang, J. Zhou, Y. Qin, C. Xu, Y. F. Hu, S. Xu, *Mater. Sci. Eng. R Rep.* **2010**, *70*, 320.

[185] a) Q. Yang, Y. Liu, C. F. Pan, J. Chen, X. N. Wen, Z. L. Wang, *Nano Lett.* **2013**, *13*, 607; b) Y. Zhang, Z. L. Wang, *Adv. Mater.* **2012**, *24*, 4712.

[186] Q. Yang, W. Wang, S. Xu, Z. L. Wang, *Nano Lett.* **2011**, *11*, 4012.

[187] C. Pan, L. Dong, G. Zhu, S. Niu, R. Yu, Q. Yang, Y. Liu, Z. L. Wang, *Nat. Photon.* **2013**, *7*, 752.

[188] L. Titova, T. B. Hoang, H. Jackson, L. Smith, J. Yarrison-Rice, Y. Kim, H. Joyce, H. Tan, C. Jagadish, *Appl. Phys. Lett.* **2006**, *89*, 173126.

[189] a) W. J. Jie, J. H. Hao, *Nanoscale* **2014**, *6*, 6346; b) Z. Y. Yin, H. Li, H. Li, L. Jiang, Y. M. Shi, Y. H. Sun, G. Lu, Q. Zhang, X. D. Chen, H. Zhang, *ACS Nano* **2012**, *6*, 74; c) W. J. Jie, Y. Y. Hui, Y. Zhang, S. P. Lau, J. H. Hao, *Appl. Phys. Lett.* **2013**, *102*, 223112; d) W. J. Jie, Y. Y. Hui, N. Y. Chan, Y. Zhang, S. P. Lau, J. H. Hao, *J. Phys. Chem. C* **2013**, *117*, 13747.

[190] a) G. Eda, H. Yamaguchi, D. Voiry, T. Fujita, M. W. Chen, M. Chhowalla, *Nano Lett.* **2011**, *11*, 5111; b) B. Radisavljevic, A. Radenovic, J. Brivio, V. Giacometti, A. Kis, *Nat. Nanotechnol.* **2011**, *6*, 147.
[191] H. L. Zeng, J. F. Dai, W. Yao, D. Xiao, X. D. Cui, *Nat. Nanotechnol.* **2012**, *7*, 490.
[192] A. Castellanos-Gomez, R. Roldán, E. Cappelluti, M. Buscema, F. Guinea, H. S. van der Zant, G. A. Steele, *Nano Lett.* **2013**, *13*, 5361.
[193] S. Wu, J. S. Ross, G.-B. Liu, G. Aivazian, A. Jones, Z. Fei, W. Zhu, D. Xiao, W. Yao, D. Cobden, *Nat. Phys.* **2013**, *9*, 149.
[194] H. J. Conley, B. Wang, J. I. Ziegler, R. F. Haglund Jr., S. T. Pantelides, K. I. Bolotin, *Nano Lett.* **2013**, *13*, 3626.
[195] Y. Hui, X. Liu, W. Jie, N. Chan, J. Hao, Y. Hsu, L. Li, W. Guo, S. P. Lau, *ACS Nano* **2013**, *7*, 7126.
[196] a) M. Allendorf, C. Bauer, R. Bhakta, R. Houk, *Chem. Soc. Rev.* **2009**, *38*, 1330; b) Y. Cui, Y. Yue, G. Qian, B. Chen, *Chem. Rev.* **2011**, *112*, 1126.
[197] a) Z. Chi, X. Zhang, B. Xu, X. Zhou, C. Ma, Y. Zhang, S. Liu, J. Xu, *Chem. Soc. Rev.* **2012**, *41*, 3878; b) F. D. Jochum, P. Theato, *Chem. Soc. Rev.* **2013**, *42*, 7468.
[198] P. Theato, B. S. Sumerlin, R. K. O'Reilly, T. H. Epps, *Chem. Soc. Rev.* **2013**, *42*, 7055.
[199] W. Z. Yuan, P. Lu, S. M. Chen, J. W. Y. Lam, Z. M. Wang, Y. Liu, H. S. Kwok, Y. G. Ma, B. Z. Tang, *Adv. Mater.* **2010**, *22*, 2159.
[200] Y. N. Hong, J. W. Y. Lam, B. Z. Tang, *Chem. Soc. Rev.* **2011**, *40*, 5361.
[201] B. J. Xu, Z. G. Chi, X. Q. Zhang, H. Y. Li, C. J. Chen, S. W. Liu, Y. Zhang, J. R. Xu, *Chem. Commun.* **2011**, *47*, 11080.
[202] a) W. Li, D. P. Yan, R. Gao, J. Lu, M. Wei, X. Duan, *J. Nanomater.* **2013**, *2013*, 14; b) J. Ni, X. Zhang, Y. H. Wu, L. Y. Zhang, Z. N. Chen, *Chem. A Eur. J.* **2011**, *17*, 1171.
[203] a) C. D. Dou, L. A. Han, S. S. Zhao, H. Y. Zhang, Y. Wang, *J. Phys. Chem. Lett.* **2011**, *2*, 666; b) C. D. Dou, D. Chen, J. Iqbal, Y. Yuan, H. Y. Zhang, Y. Wang, *Langmuir* **2011**, *27*, 6323.
[204] J. Kunzelman, M. Kinami, B. R. Crenshaw, J. D. Protasiewicz, C. Weder, *Adv. Mater.* **2008**, *20*, 119.
[205] Y. Sagara, T. Mutai, I. Yoshikawa, K. Araki, *J. Am. Chem. Soc.* **2007**, *129*, 1520.
[206] Y. Sagara, T. Kato, *Nat. Chem.* **2009**, *1*, 605.
[207] D. Yan, J. Lu, J. Ma, S. Qin, M. Wei, D. G. Evans, X. Duan, *Angew. Chem. Int. Ed.* **2011**, *50*, 7037.
[208] N. Zhao, M. Li, Y. L. Yan, J. W. Y. Lam, Y. L. Zhang, Y. S. Zhao, K. S. Wong, B. Z. Tang, *J. Mater. Chem. C* **2013**, *1*, 4640.
[209] X. C. Shan, H. B. Zhang, L. Chen, M. Y. Wu, F. L. Jiang, M. C. Hong, *Cryst. Growth Des.* **2013**, *13*, 1377.
[210] K. Okabe, N. Inada, C. Gota, Y. Harada, T. Funatsu, S. Uchiyama, *Nat. Commun.* **2012**, *3*, 705.
[211] T. Y. Han, X. Feng, J. B. Shi, B. Tong, Y. F. Dong, J. W. Y. Lam, Y. P. Dong, B. Z. Tang, *J. Mater. Chem. C* **2013**, *1*, 7534.
[212] J. W. Chung, Y. You, H. S. Huh, B.-K. An, S.-J. Yoon, S. H. Kim, S. W. Lee, S. Y. Park, *J. Am. Chem. Soc.* **2009**, *131*, 8163.
[213] M.-K. Tsang, G. Bai, J. Hao, *Chem. Soc. Rev.* 2014, DOI: 10.1039/c4cs00171k.
[214] L. Smentek, *Mol. Phys.* **2013**, *101*, 893.
[215] C.-W. Yeh, Y.-P. Liu, Z. R. Xiao, Y.-K. Wang, S.-F. Hu, R.-S. Liu, *J. Mater. Chem.* **2012**, *22*, 5828.